

A new chemistry option in WRF/Chem v. 3.4 for the simulation of direct and indirect aerosol effects using VBS: evaluation against IMPACT-EUCAARI data

P. Tuccella^{1,2,*}, G. Curci¹, G. A. Grell^{3,4}, G. Visconti¹, S. Crumeyrolle^{5,6}, A. Schwarzenboeck⁵, and A. A. Mensah^{7,}**

[1] {CETEMPS Centre of Excellence, Dept. Physical and Chemical Sciences, Univ. L'Aquila, L'Aquila, Italy.}

[2] {UPMC Univ. Paris 06, Université Versailles St-Quentin, CNRS/INSU, UMR8190, LATMOS-IPSL, Paris, France.}

[3] {Earth System Research Laboratory, National Oceanic and Atmospheric administration, Boulder, Colorado, USA.}

[4] {Cooperative Institute for Research in Environmental Sciences, University of Colorado at Boulder, Boulder, Colorado, USA.}

[5] {Laboratoire de Météorologie Physique, Université Blaise Pascal, UMR 6016, Clermont-Ferrand, France.}

[6] {LOA, UMR8518, CNRS – Université Lille1, Villeneuve d'Ascq, France }

[7] {Institut für Energie und Klimaforschung: Troposphäre (IEK 8), Forschungszentrum Jülich GmbH, Jülich, Germany}

{* now at NUMTECH, 6 allée Alan Turing, CS 60242, 63178 Aubière, France, and Laboratoire de Météorologie Dynamique, Ecole Polytechnique, 91128 Palaiseau, France}

{** now at Institute for Atmospheric and Climate Science (IAC), ETH Zurich, Zurich, Switzerland}

Correspondence to: Paolo Tuccella (paolo.tuccella@aquila.infn.it)

Abstract

A parameterization for secondary organic aerosol (SOA) production based on the volatility basis set (VBS) approach has been coupled with microphysics and radiative schemes in the WRF/Chem model. The new chemistry option called “RACM/MADE/VBS/AQCHEM” was evaluated on a cloud resolving scale against ground-based and aircraft measurements collected during the IMPACT-EUCAARI campaign, and complemented with satellite data from MODIS. The day-to-day variability and the diurnal cycle of ozone (O_3) and nitrogen oxides (NO_x) at the surface are captured by the model. Surface aerosol mass concentrations of sulphate (SO_4), nitrate (NO_3), ammonium (NH_4), and organic matter (OM) are simulated with correlations larger than 0.55. WRF/Chem captures the vertical profile of the aerosol mass concentration in both the planetary boundary layer (PBL) and free troposphere (FT) as a function of the synoptic condition, but the model does not capture the full range of the measured concentrations. Predicted OM concentration is at the lower end of the observed mass concentrations. The bias may be attributable to the missing aqueous chemistry processes of organic compounds and to uncertainties in meteorological fields. A key role could be played by assumptions on the VBS approach such as the SOA formation pathways, oxidation rate and dry deposition velocity of organic condensable vapours. Another source of error in simulating SOA are the uncertainties in the anthropogenic emissions of primary organic carbon. Aerosol particle number concentration (condensation nuclei, CN) is overestimated by a factor 1.4 and 1.7 within PBL and FT, respectively. Model bias is most likely attributable to the uncertainties of primary particle emissions (mostly in the PBL) and to the nucleation rate. Simulated cloud condensation nuclei (CCN) are also overestimated, but the bias is more contained with respect to that of CN. The CCN efficiency, which is a characterization of the ability of aerosol particles to nucleate cloud droplets, is underestimated by a factor of 1.5 and 3.8 in the PBL and FT, respectively. The comparison with MODIS data shows that the model overestimates the aerosol optical thickness (AOT). The domain averages (for one day) are 0.38 ± 0.12 and 0.42 ± 0.10 for MODIS and WRF/Chem data, respectively. Droplet effective radius (R_e) in liquid phase clouds is underestimated by a factor of 1.5, cloud liquid water path (LWP) is overestimated by a factor 1.1-1.6. The consequence is the overestimation of average liquid cloud optical thickness (COT) from few percent up to 42%. Predicted cloud water path (CWP) in all phase displays a bias in the range +41-80%, whereas the bias of COT is about 15%. In sensitivity tests where we excluded SOA, the skills of the model in reproducing the observed patterns and average values of the microphysical and optical properties of liquid and all phase clouds decreases. Moreover, the run with SOA (NOSOAA) shows convective clouds with an enhanced content of liquid and frozen hydrometers, and stronger updrafts and downdrafts. Considering that the previous version of WRF/Chem coupled

1 with a modal aerosol module predicted very low SOA content (SORGAM mechanism) the new
2 proposed option may lead to a better characterization of aerosol-cloud feedbacks.
3

1 Introduction

It is well recognized that aerosol particles have a fundamental role in the climate system. They directly alter the budget of the radiation that reaches the Earth surface by scattering and absorbing the incoming sunlight (Haywood and Boucher, 2000), and they indirectly affect cloud properties and precipitation patterns, because they act as cloud condensation nuclei (CCN) (Rosenfeld et al., 2008; Lohmann and Feichter, 2005). Some aerosol species as black and brown carbon or mineral dust heat the atmosphere absorbing the solar radiation. The local warming may increase the atmospheric stability, leading to a decrease in cloud cover through the so called semi-direct effect (Hansen et al., 1997). The global mean radiative forcing associated due to aerosols, as a result of changes in anthropogenic emissions since pre-industrial times, is highly uncertain and is estimated to be -0.9 W/m^2 , with an uncertainty range of -1.9 W/m^2 to -0.1 W/m^2 (Boucher et al., 2013).

Experimental evidence of the influence of aerosols on cloud macrophysical and microphysical properties have been shown in several works (Klarke and Kapustin, 2010; Christensen and Stephen, 2011; Koren et al., 2011; Ten Hoeve et al., 2011; Li et al., 2012). Several modelling studies show that aerosol particles have a strong impact not only on the climatic spatial-temporal scale, but also at short range on the regional scale (Baklanov et al., 2013). At regional scale, online coupled mesoscale meteorology-chemistry models are useful tools to take into account aerosol feedback effects on both meteorology and atmospheric composition (Zhang et al., 2008; Baklanov et al., 2013). WRF/Chem, which is the model used in this study, is one of such models (Grell et al., 2005; Fast et al., 2006; Chapman et al., 2009). In this work we present and evaluate some developments of WRF/Chem for a better simulation of direct and indirect aerosol feedback.

The introduction of the aerosol-cloud-radiation feedback leads to non-linear chains and loops of interactions between meteorological and chemical processes that are inhomogeneous in space and time (Baklanov et al., 2013). Furthermore, the prediction of meteorological variables significantly improves when the direct and indirect aerosol effects are taken into account in numerical simulation. For example, Yang et al. (2011) found that the inclusion of aerosol feedback produces significant benefits in the simulated optical and microphysical properties of marine stratocumulus, and these improvements positively affect the simulation of the boundary layer structure and energy budget. Yu et al. (2013) reported an improvement of the simulation of shortwave and longwave cloud forcing when the aerosol feedback is added to the model.

Recent studies conducted with global models, predict an important contribution of secondary organic aerosol (SOA) to direct and indirect aerosol feedback. O'Donnell et al. (2011) calculated an

1 annual mean direct and indirect shortwave forcing of -0.31 W/m^2 and $+0.23 \text{ W/m}^2$, respectively.
2 Biogenic SOA (BSOA) seems to play an important role on aerosol-cloud-radiation interaction.
3 Scott et al. (2014) find that BSOA contribute for 4-21% to the global annual mean of CCN and 2-
4 5% to global mean of cloud droplet concentration. They also attribute to BSOA a global mean
5 indirect radiative forcing ranges from -0.77 W/m^2 to $+0.01 \text{ W/m}^2$.
6 Previous studies over USA and Europe demonstrated that the “traditional” configuration of
7 WRF/Chem (Grell et al., 2005) using the Secondary Organic Aerosol Model (SORGAM) (Shell et
8 al., 2001), presents a negative bias of simulated $\text{PM}_{2.5}$ mass, mostly attributable to a scarce
9 production of SOA (Grell et al., 2005; McKeen et al. 2007; Tuccella et al., 2012). Therefore, an
10 updated “chemistry option” with a more sophisticated treatment of SOA, fully coupled with
11 radiative and microphysics modules, is highly desirable. In section 2 of this work, we describe the
12 developments of WRF/Chem code carried out in order to simulate the direct and indirect effects
13 with the new SOA parameterization (based on the Volatility Basis Set, VBS, approach) recently
14 implemented in the model by Ahmadv et al. (2012). In section 3, we describe the measurements
15 used to evaluate the model. In section 4, we evaluate the performance of the updated model through
16 comparison with satellite data and with meteorological and chemical constituent measurements
17 performed in the frame of the European Integrated project on Aerosol Cloud Climate and Air
18 quality interaction (EUCAARI) (Kulmala et al., 2011). The aim of the section 5 is to address the
19 two following questions: (1) Does the introduction of SOA particles interacting with radiation and
20 cloud processes improve the numerical prediction of cloud fields? (2) What is the potential impact
21 of SOA particles on cloud development? The final remarks are given in section 6.

22

2 WRF/Chem model

2.1 Description and upgrade

A pre-release of version 3.4 of Weather Research and Forecasting model with Chemistry model (WRF/Chem) (Grell et al., 2005) was used in this study. WRF/Chem is a community model that has many options for gas chemistry and aerosols. One of these has been updated in order to include a new chemistry option for simulation of direct and indirect effects with an updated parameterization for SOA production. The modifications introduced by Fast et al. (2006), Chapman et al. (2009), and Ahmadov et al. (2012) are the basis of our work. The technical details of the implementation are summarized in the Appendix A.

The gas-phase mechanism used is an updated version of the Regional Atmospheric Chemistry Mechanism (RACM) (Stockwell et al., 1997). The inorganic aerosols are treated with the Modal Aerosol Dynamics Model for Europe (MADE) (Ackermann et al., 1998). The updated parameterization for SOA production is based on the volatility basis set (VBS) approach (Ahmadov et al., 2012). MADE/VBS model has three log-normal modes: Aitken, accumulation and coarse. The species treated are the sulphate (SO_4^{2-}), nitrate (NO_3^-), ammonium (NH_4^+), elemental carbon (EC), primary organic matter (POM), secondary organic aerosol (SOA, anthropogenic and biogenic), chloride (Cl), sodium (Na), unspiciated $\text{PM}_{2.5}$ (that includes the fine fraction of sea-salt and soil dust), aerosol water, unspiciated coarse fraction of PM_{10} , soil dust and sea salt.

SOA parameterization implemented by Ahmadov et al. (2012) is based on a four bins volatility basis set, with saturation concentration of 1, 10, 100, and 1000 $\mu\text{g}/\text{m}^3$ at 300 K, respectively. VOCs are oxidized by reactions with hydroxyl radical (OH), ozone (O_3), and nitrate radical (NO_3). Oxidized VOCs are anthropogenic (alkanes, alkenes, toluene, xylene, and cresol) and biogenic (isoprene, monoterpenes, and sesquiterpenes). In each bin, organic mass is produced for two different regimes, high and low NO_x . In the former, organic peroxy radicals react with nitrogen oxide (NO), conversely in the latter organic peroxy radicals react with other organic peroxy radicals. The organic matter produced is partitioned into aerosol and gas phase assuming a pseudo-ideal partition. Organic condensation vapours (OCV) produced by the oxidation of VOCs may be oxidized by reacting with OH, consequently reducing the vapour pressure and shifting mass from high volatility bins to lower ones. The default oxidation rate (or aging factor) used in the model is $1.0 \times 10^{-11} \text{ cm}^3/\text{molec.}/\text{s}$ for both anthropogenic and biogenic OCVs. The aging factor is one the key uncertainties in SOA formation in the VBS approach. Other two factors important factors of

1 uncertainty are those related to the SOA formation pathways and to the dry deposition velocity of
2 OCVs. The latter is assumed to be 25% of the dry deposition velocity of nitric acid (HNO_3).

3 The implementation of aerosol-cloud-radiation interaction within RACM/MADE/VBS follows the
4 methods described by Fast et al. (2006) and Chapman et al. (2009). We modified the WRF/Chem
5 code by preparing the inputs for the modules devoted to calculation of the aerosol optical properties
6 and the aerosol activation, starting from the mass of each aerosol type as predicted by new
7 chemistry package. In the approach of Fast et al. (2006), the three modes of the lognormal
8 distribution are divided into 8 bins, and at each chemical constituent of the aerosol mass is
9 associated a complex refractive index. The refractive index is calculated for each bin with a volume
10 averaging. Mie theory is used to find the scattering and absorption efficiencies. Aerosol optical
11 thickness (AOT), single scattering albedo and asymmetry parameter calculated with the optical
12 package developed by Barnard et al. (2010), are used as input to the radiative scheme (Goddard and
13 RRTMG). Aerosol direct effect on longwave radiation is included following Zhao et al. (2010).

14 Aerosol-clouds interaction is a complex problem that involves the activation and resuspension of
15 the aerosol particles, aqueous chemistry and wet removal. Following Chapman et al. (2009),
16 aerosols within cloud drops are treated as "cloud borne". Aerosols that do not activate as cloud
17 droplets are treated as "interstitial". In WRF/Chem the activation process is based on the
18 parameterization developed by Abdul-Razzak et al. (2000, 2002). The number and mass
19 concentration of the activated aerosols are calculated for each mode. The activation of aerosols is
20 based on a maximum supersaturation determined from a gaussian spectrum of updraft velocities and
21 bulk hygroscopicity of each aerosol compound for all lognormal modes of particles. Bulk
22 hygroscopicity is based on the volume weighted average of the hygroscopicity of each aerosol
23 component. In addition to the activated aerosols at environmental conditions, the CCN spectrum is
24 also determined, i.e. the aerosol particles acting as CCN at some given maximum supersaturations
25 (0.02, 0.05, 0.1, 0.2, 0.5, and 1%) are calculated.

26 Within the dissipating clouds, the droplets evaporate and the cloud borne aerosols are resuspended
27 to the interstitial state. Cloud borne aerosols and dissolved trace gases may be modified by aqueous
28 chemistry. In this chemistry option, cloud chemistry is modelled using the scheme of Walcek and
29 Taylor (1986). Wet deposition of trace gases and aerosols is treated in and below clouds. Within
30 clouds the aerosols and trace gases dissolved in the water are collected by rain, graupel and snow.
31 Below clouds the wet scavenging by precipitation is parameterized using the approach of Easter et
32 al. (2004).

1 The simulation of the activation, resuspension and wet scavenging of the aerosol particles requires a
2 prognostic treatment of the cloud droplets. The prognostic treatment of the clouds droplet takes into
3 account the losses due to collision, coalescence, collection and evaporation, and the source due to
4 nucleation. The Lin and Morrison microphysics schemes in WRF/Chem version 3.4 include the
5 prognostic treatment of the cloud droplet number concentration. The source due to nucleation is
6 parameterized following Ghan et al. (1997). Both microphysical schemes take into account the
7 autoconversion of cloud drops to rain dependent on the cloud droplet number. Therefore, aerosol
8 activation affects both the rain rate and the liquid water content. The droplet number concentration
9 affects the calculation of the cloud droplet effective radius and cloud optical thickness (COT). The
10 interaction of clouds with the incoming shortwave radiation is done by linking the microphysics to
11 the radiation scheme. The reader should note that the contribution to SOA concentration by cloud
12 chemistry is missing and the interaction of aerosol with ice nuclei is not taken into account in this
13 version of the model.

14 **2.2 Model configuration**

15 The simulations were conducted over three 1-way nested domains centred on The Netherlands, as
16 shown in Figure 1. The coarse domain (D1) has 30 km horizontal resolution, domain 2 (D2) 10 km,
17 and domain 3 (D3) is cloud resolving at 2 km resolution. In our runs we used 67 vertical levels
18 extending up to 50 hPa.

19 The main physical and chemical parameterizations used are listed in Table 1. The model setup is the
20 same for all three domains, except that no cumulus parameterization is used for D3. Wet scavenging
21 and cloud chemistry from both parameterized updraft and resolved clouds are taken into account in
22 D1 and D2. However in these domains the sub-grid cloud processes involve only the interstitial
23 aerosol, i.e. the aerosol-cloud coupling is not considered in convective parameterization. Therefore,
24 the indirect effects are well resolved for domains with resolution less than 10 km in the version of
25 WRF/Chem used in this work.

26 As mentioned in Section 2.1, two key uncertainties in SOA production are deposition velocity and
27 aging factor of OCVs. The first is assumed to be 25% (this value is called “deposition factor” in
28 WRF/Chem) of dry deposition velocity of HNO_3 , the second is set to $1.0 \times 10^{-11} \text{ cm}^3/\text{molec.}/\text{s}$.
29 Ahmadov et al. (2012) showed that reducing the aging factor of OCVs by 50%, daily average
30 concentration of SOA decreases by 20%, and an increase of the dry deposition velocity of OCVs by
31 a factor 4 the SOA concentration decreases by 50%. Deposition factor and aging are tunable
32 parameters. After some sensitivity tests, we chose the default value for deposition factor and

1 $5.0 \times 10^{-11} \text{ cm}^3/\text{molec.}/\text{s}$ as aging of OCVs, because this combination minimizes the model bias with
2 observations.

3 We simulated the period from 14 to 30 May 2008. We chose this period because aerosol and cloud
4 state-of-art measurements were available to evaluate the model (see Section 3). Moreover, during
5 this period anticyclonic and cyclonic meteorological conditions were observed which allows the
6 evaluation of the model under varying conditions. The initial and boundary meteorological
7 conditions for D1 are provided by the European Centre for Medium range Weather Forecast
8 (ECMWF) analyses with a horizontal resolution of 0.5° every 6 hours. The chemical boundary
9 conditions of D1 are taken from output of the global Model for Ozone and Related Chemical
10 Tracers (MOZART) (Emmons et al., 2010). MOZART output has been converted to
11 RACM/MADE/SOA-VBS species by using the “mozbc” interface that may be downloaded from
12 the www.acd.ucar.edu/wrf-chem website.

13 A series of 30-h simulations were performed on each day starting at 00 UTC, with the first 6 h
14 discarded as model spin up for meteorology. Meteorology of D1 is reinitialized from global
15 analysis, while initial and boundary meteorology conditions for D2 and D3 are taken from D1 and
16 D2, respectively. For all three domains, the chemical initial state is restarted from previous run,
17 while the chemical boundary conditions of D2 and D3 are taken from D1 and D2, respectively. The
18 first 13 days of May 2008 are also simulated to spin-up the chemistry.

19 **2.3 Emissions**

20 Anthropogenic emissions data are taken from TNO 2007 inventory (Kuenen et al., 2014). TNO is a
21 gridded European inventory with resolution of $0.125^\circ \times 0.0625^\circ$. It provides the anthropogenic
22 emissions of NO_x , NMVOC, NH_3 , SO_2 , CO, primary $\text{PM}_{2.5}$ and PM_{10} . EC and primary OC
23 emissions are taken from a specific TNO database that is part of the EUCAARI project (Kulmala et
24 al., 2011). These EC and OC emissions are size resolved, they are separated for particles less than 1
25 μm , particles in the range of 1–2.5 μm and 2.5–10 μm .

26 Horizontal and vertical interpolation, temporal disaggregation, NMVOC speciation, and
27 aggregation of emissions into WRF/Chem species is done following Tuccella et al. (2012), with
28 minor updates described in Curci et al. (2014a). In order to prevent spurious concentration of
29 aerosol particles, the distribution of aerosol emissions into WRF/Chem modes is based on the low
30 emission scenario of Elleman and Covert (2010). The 10% of the emitted aerosol mass is attributed
31 to Aitken mode, and the 90% to the accumulation mode.

1 Biogenic emissions are calculated on line with Model of Emissions of Gases and Aerosols from
2 Nature (MEGAN) (Guenther et al., 2006). Dust and sea salt emissions from soil and seawater are
3 calculated on line in the simulations.
4

3 Measurements

We evaluated model performances in D3 against ground and aircraft based data collected in May 2008 during the Intensive Cloud Aerosol Measurement Campaign (IMPACT) in the frame of the EUCAARI project (Kulmala et al., 2009). Model results were also evaluated against MODIS satellite data.

An overview of the synoptic conditions of May 2008 over Central Europe is given by Hamburger et al. (2011). The first 15 days of May are characterized by an anticyclonic block, while the period from 16 to 31 is dominated by westerly wind and passage of several fronts. The days from 17 to 20 May are referred as “scavenged background situation” (Mensah et al., 2012), because they are dominated by northerly wind from North Sea associated to a low aerosol mass loading, due to wet scavenging. The period starting from 23 May is dominated by long range transport of dust from Sahara desert (Roelofs et al., 2010; Begue et al., 2014).

3.1 Ground based measurements

Meteorological and aerosol ground based measurements used in this study are collected in Cabauw (The Netherlands) at CESAR observatory Cabauw (Figure 1). CESAR observatory is a tower located at 51° 57'N, 4° 54' E, and -0.7 m a.s.l, at about 50 km south of Amsterdam. Measurements performed at CESAR observatory are typical of North-West Europe, and are representative of maritime and continental conditions depending on the wind direction (Mensah et al., 2012).

Standard meteorological variables are collected at 2 m, 10 m, 20 m, 40 m, 80 m, 140 m, and 200 m height. Besides, in this study we used the measurements of temperature and relative humidity profiles obtained with radiometer, and aerosol speciation from aerosol mass spectrometry (AMS) collected at 60 m (Mensah et al., 2012).

The model is also compared to ozone (O_3), nitrogen oxide (NO_x), nitric dioxide (NO_2), nitric oxide (NO), ammonia (NH_3), nitric acid (HNO_3), nitrous acid ($HONO$), and sulphur dioxide (SO_2) measurements issued by Cabauw Zijdeweg EMEP station (NL0011R). O_3 is measured with an ultraviolet absorbing ozone instrument, NO_x , NO and NO_2 with a chemiluminescence monitor, and NH_3 , HNO_3 , $HONO$ and SO_2 with an online ion chromatograph.

Although Cabauw supersite provides very detailed measurements, it could not be enough to characterize the model performance near the surface. Therefore, WRF/Chem is also compared to daily PM_{10} data from 63 stations (10 rural, 25 suburban, and 28 urban) of AIRBASE network and to daily inorganic aerosol measurements issued at Bilthoven (NL0008R), Kollumerward (NL0009R),

1 Vredepeel (NL00010R), and De Zilk (NL00091R) EMEP stations. SO_4 and NH_4 measurements are
2 also performed at all these sites while NO_3 measurements are available only at De Zilk.

3 **3.2 Aircraft measurements**

4 During May 2008, the French ATR-42 research aircraft performed 22 research flights (RF). In this
5 work we used 14 RF to evaluate the model. Their tracks are reported in Figure 1, while flight
6 number, take-off and landing time are reported in Table S1. RF50, RF55, RF56, RF57, RF58, RF61
7 and RF62 were conducted around Cabauw supersite, in order to study the origin and characteristic
8 of air masses collected at Cabauw. Other RFs were aimed at the study of aerosol properties along a
9 quasi-Lagrangian flight track, with west-east and north-south transects. ATR-42 was equipped with
10 instrumentation suitable for aerosol-cloud interaction measurements. We used the measurements
11 from a condensation particle counter (CPC), the CPC3010 with a cutoff size of 15 nm, a Cloud
12 Condensation Nuclei Counter (CCNC) for CCN number concentration measurements, and an AMS.
13 During the campaign a scanning mobility particle sizer (SMPS) was used to measure the number
14 size distribution of aerosol particles with diameter in the range of 0.02-0.5 μm , while the size
15 distribution of aerosol particles larger than 100 nm was sampled with a passive cavity aerosol
16 spectrometer probe (PCASP). SMPS and PCASP measurements were combined in order to
17 calculate the $\text{PM}_{2.5}$ concentration using an average aerosol density of 1.7 g/m^3 . A more exhaustive
18 and detailed description of the whole campaign and instrumentation is given by Crumeyrolle et al.
19 (2013).

20 **3.3 Satellite measurements**

21 The model was also evaluated with MODIS-Aqua aerosol and cloud data. The Level 2 products
22 used here are MYD04 and MYD06 collection 051 for aerosol and clouds, respectively. For ease of
23 comparison with model output, both satellite and model data were regridded onto a common lat-lon
24 regular grid. Model output is sampled at same time and location of each MODIS pixel, and then
25 data are averaged in space and time over the same grid. In this study the horizontal spacing of the
26 common grid is 4 km.

27

1 **4 Model evaluation**

2 Model results are compared to ground based and aircraft observations, as detailed in section 3. The
3 statistical indices used are the Pearson's correlation coefficient (r), mean bias (MB), normalized
4 mean bias (NMB) and normalized mean gross error (NMGE). The indices are defined in the
5 Appendix and reported in Table 2.

6 **4.1 Meteorology**

7 Figure 2 shows the observed and modelled time series of hourly vertical profiles of temperature and
8 relative humidity at Cabauw supersite. WRF/Chem reproduces the day-to-day variation of
9 temperature, before, after, and during the wet period. As shown by statistical indices (Table 2),
10 within the first 200 m, the model reproduces the temperature with a correlation of 0.93-0.95 and a
11 mean bias of about -0.5°C . Looking at the free troposphere, we may realize that the model
12 underestimates the height of the 0°C isotherm (the black line on Figure 2a) in the first days of
13 simulation and during wet period by about 200-300 m (i.e., the model is colder than observed by 1-
14 1.5°C). Whereas immediately after the passage of the cold front, the temperature rise in the
15 simulation is slower than the observed one. The model performances in simulating surface
16 temperature are consistent with other European studies (e.g., Zhang et al., 2013a; Brunner et al.,
17 2014). For example, Brunner et al. (2014) compared several meteorology-chemistry coupled models
18 with annual simulations at continental scale, and found that on Central Europe the predicted surface
19 temperature shows a correlation with observations in the range of 0.95-0.98, whereas the bias
20 ranges from -1 to 0.1°C .

21 The model reproduces the vertical structure of relative humidity (Figure 2b) over the whole period,
22 but it has the tendency to overestimate (underestimate) the higher (lower) observed values. This
23 behaviour is more evident during scavenging days, when the relative humidity between 1000-2000
24 m is overestimated on average by 40%, but sometimes up to 60%. Errors of this magnitude in
25 simulating the vertical profile of RH were already found in previous works (Misenis and Zhang,
26 2011; Luo and Yu, 2011). Nevertheless, the model correlation and mean bias are 0.84 and +3.4%
27 below 1000 m of altitude, 0.50 and +13% in the range of 1000-2000 m, 0.78 and +6.4% between
28 2000-3000 m. These values are comparable with those found by Fast et al. (2014) in the comparison
29 of WRF/Chem simulations to aircraft data. They have shown correlations in the interval of 0.49-
30 0.70, while the bias from -7 to +0.1%. Near the surface, the relative humidity is simulated with a
31 correlation of 0.87-0.92 and a positive MB of 3-4% (+6-8%).

1 The biases of the temperature and relative humidity could be due to a misrepresentation of soil (and
2 sea) temperature and soil moisture or by misrepresentation of the clouds and rain. These two
3 problems are tightly coupled via land surface-atmosphere interaction. The errors in the simulation
4 of surface moisture and energy budget influences the fluxes of latent heat and moisture in the
5 atmosphere, affecting the local circulation, convective available potential energy (CAPE), cloud
6 formation and rain pattern (Pielke, 2001; Holt et al., 2006). Moreover, WRF/Chem tends to fail
7 simulating the thermodynamic variables near to coastline, because the uncertainties of land use data
8 may play an important role (Misenis and Zhang, 2010). Initial and boundary meteorological
9 conditions may also play an important role. Bao et al. (2005) demonstrated that meteorological
10 prediction is sensitive to used input data. They showed that varying the inputs used as initial and
11 boundary conditions, the mean daily model bias ranges from -2.71 to -0.65 K for the temperature
12 and from -0.81 to 0.50 g/kg for vapour water content.

13 In Figure 3 we compare the time series of observed and predicted wind speed and direction at
14 several heights of Cabauw Tower. WRF/Chem captures the diurnal trend of wind speed, but it
15 overestimates the wind speed during night. Generally, we found the higher correlation at 10 and 200
16 m (0.78 and 0.76 respectively) and higher NMB between 20 and 40 m (+30-40%). The wind
17 direction is captured at all altitude levels of Cabauw tower, except of 18May when WRF/Chem
18 does not reproduce some rapid variations most likely due to local effects. The simulation of wind
19 direction tends to improve with height. Indeed, the correlation coefficient increases from 0.52 to
20 0.73 at 10 and 200 m, respectively, and the MB decreases from 27° below 40m to 17° at 200 m. The
21 performance in simulating the surface wind speed are consistent with those reported by Brunner et
22 al. (2014) in Central Europe. They have shown a correlation for 10 m wind speed in the range of
23 0.53-0.73 and a mean bias of 1-1.8 m/s. It is well recognized that WRF tends to overestimate the
24 wind near the surface (e.g. Misenis and Zhang, 2010; Ngan et al., 2013; Brunner et al., 2014), but
25 the bias of the simulated wind speed could be also explained with uncertainties in the large-scale
26 pattern of analysis used as input. Bao et al. (2005) showed that varying the meteorological inputs,
27 the mean daily model bias may range from -1.53 to -0.28 m/s and from -1.43 to 0.01 m/s for the u
28 and v component of the wind, respectively.

29 **4.2 Surface gas phase and aerosol mass**

30 Figure 4 displays the comparison between the observed and modelled hourly time series and
31 average diurnal cycles of O₃, NO_x, NO₂, NO, NH₃, HNO₃, HONO and SO₂ near the surface.

1 WRF/Chem reproduces the day to day variations of O_3 , capturing its decrease during scavenging
2 period due to low photolysis rate caused by cloud presence, recovery in the following days, and a
3 new decrease starting from 25 May. The average daily cycle is well reproduced with a morning
4 minimum and an underestimated maximum in the afternoon. The model simulates the O_3 with a
5 correlation of 0.72 and systematic negative bias on average about $3.4 \mu\text{g}/\text{m}^3$. This bias is observed
6 in the afternoon and the evening, and is most likely due to the titration in these hours caused by
7 higher NO_x concentration than observed.

8 WRF/Chem simulates the NO_x , NO and NO_2 time series with a correlation of 0.70, 0.65, and 0.66
9 respectively. The timing of NO_x daily cycle is reproduced. Indeed, the model captures the morning
10 and evening peaks as well as diurnal minimum of NO_2 . The mean bias of modelled NO_2 is $+1.25$
11 $\mu\text{g}/\text{m}^3$ (+20%) and occurs in the afternoon and evening hours. Moreover WRF/Chem reproduces the
12 morning peak and diurnal decrease of NO , but the daily cycle is affected by an average positive bias
13 of $0.28 \mu\text{g}/\text{m}^3$, with the average morning maximum overestimated of about $2 \mu\text{g}/\text{m}^3$ (+33%).

14 Ammonia is reproduced with a correlation of 0.43. WRF/Chem underestimates the NH_3 during the
15 scavenging days and from 28 to 31 May. The model captures the daily cycle shape of NH_3
16 concentration average, but the modelled NH_3 concentrations are constantly underestimated. The
17 negative mean bias over the whole period is on average about $-4.75 \mu\text{g}/\text{m}^3$ (-28%). WRF/Chem
18 reproduces the observed HNO_3 with a poor correlation. The measured mean diurnal cycle is flat,
19 conversely the model predicts a nocturnal minimum and diurnal maximum. The origin of model
20 bias in simulating NH_3 and HNO_3 is discussed below, together with a discussion on inorganic
21 aerosols.

22 The nitrous acid concentrations are not well captured by the model and are underestimated by 95%.
23 This bias could be partly explained by the inefficiency of NO oxidation, the only important reaction
24 known to form HONO . Lin et al. (2014), indeed, demonstrated that the major sources of HONO are
25 some unknown reactions that consume nitrogen oxides and hydrogen oxide radicals.

26 The model reproduces the measured SO_2 with a correlation of 0.48 and a positive bias of 0.68
27 $\mu\text{g}/\text{m}^3$ (+90%). The overprediction is most likely attributable to anthropogenic emissions. SO_2 is
28 emitted mainly from isolated and elevated large point sources (Figure S1) that are immediately
29 mixed in the model cell leading to overestimation outside of the local plume (Stern et al., 2008).
30 This is demonstrated, for example, by the larger NMGE for SO_2 than NO_x (116% and 45%,
31 respectively). NO_x is emitted near the surface by traffic and domestic heating. Therefore, NO_x
32 emissions are subjected to a stronger temporal modulation than SO_2 point sources.

1 The different uncertainties found for the involved species may depend on the choice of the chemical
2 mechanism. Knote et al. (2014) compared several chemical mechanisms within a box model
3 constrained by the same meteorological conditions and emissions, and found that the prediction of
4 the O₃ diurnal cycle differs by less than 5% among the different mechanisms. Larger differences
5 were found for other species. For example, the key radicals exhibit differences up to 40% for OH,
6 25% for H₂O₂ and 100% for NO₃ among the selected mechanisms.

7 Figure 5 shows the simulated and observed time series and diurnal cycle of aerosol sulphate, nitrate,
8 ammonium, and organic matter, at CESAR observatory. WRF/Chem simulates the measured SO₄,
9 NO₃, NH₄ with a correlation of 0.56, 0.68, and 0.66, respectively.

10 WRF/Chem captures the daily variations of SO₄ and its decrease during scavenging days. The shape
11 of diurnal cycle is also reproduced, with the nighttime minimum and diurnal maximum. The mass
12 concentration of SO₄ is overpredicted for the whole period with a mean bias of 1.04 µg/m³ (+90%).
13 The modelled SO₄ overestimation is directly attributable to SO₂ concentration overprediction.
14 Another potential source of the surplus of simulated SO₄ is related to an excessive production
15 within the clouds. Indeed, during scavenging days, the particulate sulphate is overestimated while
16 the predicted SO₂ does not show a bias in respect to the measurements. The overestimation of SO₄,
17 moreover, explains in part the negative bias of predicted NH₃. The excess of particle sulphate
18 consumes too much ammonia (Meng et al., 1997)

19 NO₃ is reproduced with a positive bias of 1 µg/m³ (+72%). Looking at diurnal cycle, the modelled
20 nitrate is on average biased high in the daytime, with a peak in the afternoon. This maximum
21 appears to be correlated with HNO₃ maximum. Really, the HNO₃ peak is caused by evaporation of
22 particulate nitrate formed in the upper PBL (where the conditions of lower temperature and higher
23 relative humidity are favourable to NO₃ formation), and mixed towards the surface by vertical
24 mixing (Curci et al., 2014a; Aan de Brugh et al., 2012). Therefore, the unrealistic afternoon peak of
25 modelled nitric acid should result from a too rapid relaxation of aerosol-gas partitioning to
26 thermodynamic equilibrium (Aan de Brugh et al., 2012).

27 The behaviour of the simulated NH₄ is related to modelled trend of NO₃. It is biased high by 0.66
28 µg/m³ (+66%). The NH₄ overestimation is related to NH₃ underprediction (Meng et al., 1997).

29 Similar performances are found in reproducing inorganic aerosols at other Dutch EMEP sites (see
30 Section 3.1). Daily SO₄ is simulated with an average correlation (3 stations) of 0.66 and a positive
31 bias of 35%. WRF/Chem simulates NH₄ with a correlation of 0.82 (4 stations) and a bias of +43%.
32 Predicted daily NO₃ (measured at only one station) is overestimated by 15%.

1 Organic matter is reproduced with a correlation coefficient of 0.75. WRF/Chem reproduces the
2 right concentration during dry period, the decrease in the wet days, and following recovery. The
3 mean bias is negative by about $0.4 \mu\text{g}/\text{m}^3$ and it is attributable to days from 23 to 26 May. The
4 discussion about the origins of OM bias is given in section 4.3, where we will discuss the model
5 evaluation with aircraft data.

6 The reader should consider that aerosol composition measurements performed with the AMS are
7 representative of particles with diameter between roughly 100-700 nm, whereas the model is
8 evaluated with aerosol concentration representative of $\text{PM}_{2.5}$. Therefore, a bias could be present in
9 the comparison. This means that the bias found for inorganic aerosols could be smaller than that
10 reported above, conversely the OM bias could be larger of that found.

11 The model evaluation performed so far is representative of few points in the domain and does not
12 include other aerosol components like black carbon or primary PM. This could limit our
13 understanding of the model behaviour. In order to overcome this shortcoming, WRF/Chem is also
14 compared to daily PM_{10} measurements of AIRBASE network (Figure S2). The model captures the
15 daily variations of PM_{10} , the PM_{10} decrease during scavenging days, the consequent recovery to
16 reach back the background PM_{10} concentration and the PM_{10} enhancement during long-range
17 transport period. Indeed, the correlations are of 0.72, 0.73, 0.75 in rural, suburban, and urban zones,
18 respectively. Model bias at rural stations is important in the last days of May 2008, indeed in these
19 days (28-30 May) it is about $-15 \mu\text{g}/\text{m}^3$ (-30%). Conversely, at suburban and urban stations, the
20 model presents a bias for the most part of the days of about $3\text{-}4 \mu\text{g}/\text{m}^3$ (5-10%) that could partly
21 explained by the missing source of resuspension due to traffic.

22 The results obtained here are statistically consistent with other modelling studies over Europe (e.g.,
23 Lecœur and Seigneur, 2013; Zhang et al., 2013b; Balzarini et al., 2014). For example, the results of
24 European annual simulations of Balzarini et al. (2014) exhibited a correlation of 0.48, 0.60 and 0.56
25 for surface SO_4 , NO_3 and NH_4 , respectively. During EUCAARI campaign, Athanasopoulou et al.
26 (2013) reported a mean correlation of surface OM with observations of 0.56 and a mean bias of -0.5
27 $\mu\text{g}/\text{m}^3$, whereas Fountoukis et al. (2014) simulates the OM at Cabauw on May 2008 with a bias of
28 $0.3 \mu\text{g}/\text{m}^3$. Moreover, with regards to surface PM_{10} , our performances are comparable to those
29 found for example by Im et al. (2014) over Europe with annual simulations in terms of correlation,
30 but are higher in terms of bias. Comparing PM_{10} concentrations from several models, Im et al.
31 (2014) found correlations of 0.18-0.86 and 0.07-0.82, and bias of about -40% and -50% for rural
32 and urban sites, respectively. This improvement is most likely due to the very high resolution used

1 in this study with respect to the 23 km of Im et al. (2014), since the anthropogenic emissions
2 inventory used is the same here and in Im et al. (2014) study.

3 **4.3 Aloft aerosol mass concentration**

4 The comparison of WRF/Chem to aircraft data is done interpolating the model output point by point
5 along the flight track. Observed and modelled aircraft data are presented by using the box plots for
6 planetary boundary layer (PBL) and free troposphere (FT) (see Figure 6). The height of the PBL
7 was lower than 1600 m during the whole campaign (Crume rolle et al., 2013). Therefore, we
8 considered for PBL and FT concentrations the data below and above 1600 m up to 3000-4000 m,
9 respectively. This rough approximation of PBL height could affect the comparison of the model to
10 data.

11 Figure 6 displays the observed and modelled box plots of the mass concentration of SO₄, NO₃, NH₄,
12 and OM for PBL and FT. Their mean value, standard deviation, relative mass fraction, and
13 correlation coefficients, averaged over the whole period of interest, are reported in Table 3.

14 The average concentrations of inorganic aerosols show little absolute error (2-8%) with respect to
15 the observations in the PBL, while the NO₃ and NH₄ mean concentration presents a bias of +14%
16 and +20% (+0.3 and +0.2 µg/m³), respectively, in the FT. The mean OM mass is biased low by a
17 factor 2 and 3 in the PBL and FT, respectively. The correlation coefficients of SO₄, NO₃, NH₄, and
18 OM are 0.39, 0.47, 0.43, 0.67 in the PBL and 0.23, 0.44, 0.42, 0.53 in the FT. These performances
19 are comparable with those found with WRF/Chem (but with a different chemistry package) in
20 California by Fast et al. (2014). They reported an absolute mean bias of about 0.01-0.2, 0.03-0.6,
21 0.1-0.45, 0.2-0.57 µg/m³ and a mean correlation of 0.42, 0.45, 0.44, and 0.72 for SO₄, NO₃, NH₄,
22 and OM, respectively.

23 Although the predicted aerosol mass of each species is within the range of the observed values for
24 most of the flights used in this study (see Figure 4), the model does not capture the full range of the
25 measured concentrations. This assertion is made quantitative by the standard deviations reported in
26 Table 3. The predicted standard deviations for each species are lower than observed. In the PBL, the
27 observed and modelled standard deviations differ by 4-10% for inorganic ions and 55% for OM. In
28 the FT, the differences are higher than in the PBL. The model predicts standard deviations lower
29 than 10-40% for inorganic particles and lower than 65% for organic matter with respect to the
30 measurements.

31 For the purpose of this analysis, it is also interesting to explore how the model reproduces the
32 relative fraction of aerosol mass species with altitude (see Table 3). WRF/Chem overpredicts the

1 relative fraction of the SO_4 and NO_3 by few percent in the PBL and about 10% in FT, while the
2 relative mass of NH_4 is overestimated by 3% along the whole profile. The relative amount of OM is
3 underpredicted by about 20% in both PBL and FT. The decrease of relative amount of NO_3 and
4 increase of SO_4 with altitude is captured by the model. The modelled relative mass of NH_4 and OM
5 is near constant with altitude as well as in the observations.

6 Looking at the individual flights, it is possible to note how the model captures the aerosol mass
7 trend as a function of the synoptic frame in both the PBL and FT, during the dry period, scavenging
8 days, and dust period characterized by southerly wind and passage of several fronts. The FT is a
9 layer mainly affected by long range transport and cloud contamination. Therefore, the relative small
10 bias in simulating aerosol inorganic mass in FT means that the model resolves quite correctly the
11 large scale transport and processes related to clouds.

12 Nevertheless, it should be noted that SO_4 is overestimated for 8 out of 14 RFs, while NO_3 and NH_4
13 are underpredicted for 7-8 out of 14 RF. This SO_4 overprediction is attributable to the SO_2 excess
14 and to a potential overproduction within the cloud chemistry scheme. The negative bias of NO_3 and
15 NH_4 could be explained by a low NH_3 regime, that limits the formation of the ammonium-nitrate.

16 The simulated OM concentration is always at lower end of the observed variability. Several factors
17 may explain this systematic bias. First of all, our simulations do not include the processing of
18 organic compounds in aqueous chemistry. SOA may be produced in the clouds (Hallquist et al.,
19 2009). Modelling studies suggest that the contribution of cloud chemistry to SOA budget is almost
20 as much as the mass formed from the gas phase (Ervens et al., 2011). OM prediction is also affected
21 by meteorological errors. Bei et al. (2012) found that the uncertainties in meteorological initial
22 conditions have significant impact on the simulations of the peaks, horizontal distribution and
23 temporal variation of SOA. The same authors demonstrated that the spread of the simulated peaks
24 can reach up to $4.0 \mu\text{g}/\text{m}^3$. Other uncertainties may be related to the VBS formulation. SOA
25 formation pathways is one these, indeed halving the SOA yields the concentration of SOA
26 decreases by 30% (Ahmadov et al., 2012). Moreover, the assumption on the deposition velocity of
27 the OCVs may play an important role in the uncertainties of SOA production. The OCV deposition
28 velocity in the version of the VBS implemented in WRF/Chem by Ahmadov et al. (2012) is
29 proportional to the deposition velocity of the HNO_3 . The proportionality constant is a tunable
30 parameter and in this work is set to the default value of 0.25. WRF/Chem prediction of SOA mass
31 is very sensitive to the choice of the proportionality constant (Ahmadov et al., 2012). Previous
32 studies have shown that SOA concentration is highly sensitive to the treatment of the deposition
33 velocity of OCV (Bessagnet et al., 2010; Knote et al., 2014b). Finally we note that OM bias could

1 be partially explained by the uncertainties in the anthropogenic emissions (e.g. bias or spatial
2 distribution) of primary organic carbon and in the factor 1.6 used to convert them to primary OM
3 (POM) (Turpin and Lim, 2001). The reader should also consider that the uncertainties in POM
4 simulation affect the SOA formation. Indeed, the partition between OCV and SOA used in VBS
5 approach depends on the total OM (Equation 1 of Ahmadov et al., 2012), thus if POM is
6 underpredicted the resulting SOA could be underestimated.

7 In order to have a more complete overview of the model skill in reproducing the upper air aerosol
8 mass concentration, we compare also the observed and modelled $PM_{2.5}$. Figure 7 shows measured
9 and predicted box plots of the $PM_{2.5}$ concentration in PBL and FT. Modelled $PM_{2.5}$ is in the range
10 of the observed values within the PBL except during wet scavenging period when it is at the lower
11 end of the observations. In FT conversely, predicted $PM_{2.5}$ is at the lower end of the observed
12 profiles for the most part of the flights. The comparison between modelled and observed $PM_{2.5}$
13 concentration within PBL and FT show good correlations (0.75 and 0.80, respectively).

14 Model correlation with observations is high, 0.75 and 0.80 in PBL and FT, respectively. The
15 absolute mean bias is of $-7 \mu g/m^3$ (30-35%) in both PBL and FT.

16 Although the box plot and statistical summary (Table 3) provide significant information on the
17 model performances, the model skills in reproducing vertical profiles of aerosol properties need to
18 be evaluated. Therefore, we also look at model vertical profiles along the flight tracks. As an
19 example, we have chosen the 14 May 2008 (RF50) for two reasons: first, there is a relatively large
20 contribution of OM, SOA (70-85% of OM), and CCN (see Figure 10), and second, it is a day of
21 high pressure, thus the interpretation of the results is not complicated by cloud processes. Figure 8
22 displays the comparison of modelled vertical profiles of $PM_{2.5}$, SO_4 , NO_3 , NH_4 and OM along the
23 flight track and measurements. WRF/Chem captures several features present in the aircraft
24 observations. Both observed and modelled $PM_{2.5}$ exhibit a maximum in a layer between 500 and
25 about 2000 m. Model predicts the inhomogeneity of chemical secondary species of $PM_{2.5}$ displayed
26 also in the observations: SO_4 and OM concentrations are relatively homogeneous within the PBL,
27 whereas NO_3 and NH_4 show enhanced concentrations in the upper levels of the PBL. For
28 completeness, we note that primary $PM_{2.5}$ components (not shown) have the maximum close to the
29 surface (first 500 m) and are diluted throughout the PBL. These results are qualitatively similar to
30 those found by Curci et al. (2015) above Milan (Italy).

1 **4.4 Aloft aerosol particles**

2 The comparison of WRF/Chem output with aircraft measurements of the number concentration of
3 condensation nuclei (CN) and of cloud condensation nuclei (CCN) at 0.2% of supersaturation is
4 done by using the boxplots as for aerosol mass. In this case the modelled and measured data are
5 smoothed by using a 10 seconds running mean.

6 Figure 9 reports the comparison of observed and modelled CN within PBL and FT. The measured
7 and predicted average, standard deviation, and correlation of CN number over the whole period of
8 our analysis are reported in Table 3.

9 The model resolves the decrease of a factor 5-6 of CN concentration between the PBL and the FT.
10 The differences in simulated concentrations between land and sea (RF51 and 52) are also captured
11 by the modelling system. Nevertheless, WRF/Chem overestimates, on average, the observed CN by
12 a factor 1.4 within PBL and 1.7 within the FT. The bias is less pronounced above the sea during the
13 (RF51 and RF52), where the anthropogenic sources are less important. Moreover, it should be noted
14 that in some cases, for example during the RF56, 57 and 58, the predicted CN are completely
15 outside the range of the observed values. In these cases the predicted CN are biased high by about a
16 factor of 2-3. Predicted CN concentration shows a higher variability than measured, especially in
17 the free troposphere where the difference of modelled standard deviation is biased high by 155%.
18 Anyway, the modelled CN concentration correlates well with the observed one (0.40 and 0.74 in
19 PBL and FT, respectively). These values are consistent with the 0.61 found by Luo and Yu (2011)
20 studying the new particle formation and its contribution to CN with a version of WRF/Chem
21 including an advanced aerosol microphysical model.

22 Figure 10 shows the comparison of observed and modelled CCN at 0.2% of supersaturation. The
23 measured and predicted average and standard deviation of CCN are showed in Table 3. The bias of
24 simulated $CCN_{0.2}$ appears more contained with respect to CN prediction, especially in the free
25 troposphere. Figure S3 shows the comparison of the modelled vertical profile of CCN along the
26 flight track of 14 May and observed CCN aboard the ATR42. WRF/Chem predicts relatively
27 homogeneous profile of CCN in the PBL also shown by observations.

28 The aerosol particles that mostly contribute to CCN number are those of accumulation and coarse
29 modes, and accumulation and coarse mode particles are also the major contributor to $PM_{2.5}$ mass
30 concentrations. Since $PM_{2.5}$ is underestimated and CCN overestimated, CCN bias cannot depend on
31 model errors in $PM_{2.5}$. The major uncertainties in predicted CCN arise from aerosol nucleation rate
32 and primary emissions (Lee et al., 2013). Direct emission of aerosol particles is the key factor for
33 CCN production in the PBL and near particle sources (Spracklen et al., 2006), and account for 55%

1 of the total global production (Merikanto et al., 2009). On the other hand, nucleation and
2 subsequent growth up to CCN size is an important mechanism of CCN formation in many parts of
3 the atmosphere (Sotiropoulou et al., 2006). Using several nucleation parameterizations, Pierce and
4 Adams (2009) showed that CCN on average varies by up to 12% within the PBL. At the same time,
5 they also found that varying by a factor of 3 the primary emissions, the CCN mean changes by 40%
6 in the PBL. On the basis of these argumentations and the correlation between predicted and
7 observed CN being larger in the FT than in PBL (i.e. far from anthropogenic sources), we may
8 speculate that the errors in the CCN prediction arise mainly from the uncertainties in the primary
9 emissions of the aerosol particles and in their distribution in the lognormal modes.

10 The analysis of CCN efficiency reveals other interesting features in the model behaviour. The CCN
11 efficiency is given by CCN/CN ratio and represents the ability of aerosol particles to nucleate cloud
12 droplets (Andreae and Rosenfeld, 2008). CCN efficiency observed during the studied RFs is in the
13 range of 0.02-0.33 for PBL and 0.18-0.41 in the FT, while the model predicts values of 0.03-0.17
14 and 0.04-0.18 for PBL and FT, respectively. In other words, WRF/Chem underestimates the CCN
15 efficiency by a factor of 1.5 and 3.8 within the PBL and FT, respectively. Moreover, the modelled
16 CCN efficiency, contrary to the observation, shows almost the same range of values within the PBL
17 and within the FT.

18 The so calculated and modelled CCN efficiencies could be underestimated. In general, the CCN
19 efficiency should be computed with the aerosol population with size larger than the minimum
20 activation diameter (Asmi et al., 2012). The latter depends on the aerosol type and ranges from
21 about 50 to 125 nm. We calculated the observed CCN/CN ratio with the measurements of CPC
22 3010 which gives the total number of particles larger than 15 nm, and modelled CCN fraction is
23 calculated with total particle number given by the sum of the three modes of the lognormal
24 distribution (Aitken, accumulation and coarse). In order to better characterize the relationship
25 between CCN and corresponding aerosol population in the model, predicted CCN efficiency was
26 also calculated with particles of the accumulation and coarse modes (the most favored particles to
27 act as CCN) and it was qualitatively compared to observed efficiency during the IMPACT
28 campaign computed with particles larger than 100 nm. Observed values of CCN efficiency are in
29 the range of 0.28-0.4 and 0.38-0.6 in the PBL and FT (Crumeyroille et al., 2013), respectively. The
30 simulated CCN fraction calculated with the particles of the accumulation and coarse modes, is
31 always underestimated with respect to the observations, and it is in the range of 0.17-0.3 in PBL and
32 0.23-0.36 in FT. The model deficiency in simulating the CCN/CN ratio could be attributable to the

1 uncertainties in geometrical diameter and bulk hygroscopicity of the lognormal modes, and updraft
2 velocity that lead to error in the prediction of minimum activation diameter of each mode.

3 **4.5 Comparison with MODIS data**

4 WRF/Chem output was also compared to aerosol optical thickness (AOT), cloud microphysical and
5 optical properties retrieved by MODIS-Aqua.

6 Figure 11 shows the comparison between the AOT at 550 nm measured by MODIS and the
7 corresponding AOT predicted by the model during the high pressure period on 14 May 2008.
8 WRF/Chem reproduces the spatial distribution of observed AOT, such as the lowest values in the
9 southern part of the domain or the highest values around Cabauw, but underestimates the strong
10 gradient between eastern boundary and the centre of the domain. The model overestimates the
11 regional mean of AOT, indeed the domain averages are 0.38 ± 0.12 and 0.42 ± 0.10 for MODIS and
12 WRF/Chem data, respectively. Unfortunately, good coverage of the D3 domain by MODIS was
13 achieved only on one day (14 May 2008), this does not allow us to have a general overview of
14 model skill in predicting AOT. In general, model intercomparisons revealed that a large part of the
15 uncertainties in simulating the AOT arises from the assumption on the mixing state. For example,
16 AOT computed with external mixing is larger by 30-35% of that calculated with internal mixing
17 assumption (Curci et al., 2014b). For typical atmospheric particle sizes and in the visible
18 wavelength range, the AOT is then expected to be lower under internal mixing assumption (that is
19 the assumption done in this work). Moreover, a 10% error in predicting AOT may be attributable to
20 the choice of species density, refractive index, and hygroscopic growth factor (Curci et al., 2014b).

21 As the WRF microphysics scheme accounts for aerosols only within liquid clouds, comparison
22 among predicted cloud optical and microphysical properties with MODIS data was done separately
23 for liquid, excluding mixed clouds. Top liquid cloud effective radius (R_e) was calculated from
24 liquid water content (LWC) and cloud droplet number concentration predicted by WRF/Chem.
25 Liquid water path (LWP) was calculated by vertically integrating liquid cloud mixing ratios (water
26 and rain water), while liquid cloud optical thickness (COT) was estimated from LWC and R_e . Since
27 MODIS L2 data provide the total cloud water path (CWP), combined effective radius for all cloud
28 types and total (water and ice) cloud optical thickness (COT), the observed contribution to the
29 liquid water cloud was separated by using the retrieved top cloud phase, i.e. were discarded mixed
30 clouds.

31 The comparison between the predicted and observed R_e , LWP and liquid COT was done in the
32 scavenging background and long-range transport periods in the days when MODIS cloudy pixel

1 coverage was larger than 60%. Figure 12 shows the comparison of the averaged values for 17-19
2 May 2008 period (1P). The same comparison has been done on averaged values for 25-27 (2P) and
3 28-30 May (3P) and are reported in the Supplement (Figures S4 and S5). WRF/Chem reproduces
4 several features of the liquid cloud systems during 1P: the liquid cloud distribution, the maximum
5 values of R_e close to the coast, maximum of LWP and liquid COT on the centre and at **North-East**
6 of the domain. However, model results present a larger spatial extension of liquid water cloud
7 highest values off the Dutch and Belgian coast not observed in the MODIS data. During 2P the
8 structure of the cloud system is not completely reproduced by the model. Although R_e value
9 magnitude is captured above the sea, WRF/Chem underestimates the cloud droplet dimension on
10 the land. Therefore LWP and liquid COT structure on the sea is resolved by the model, whereas on
11 the land they are too small compared to the observations. Finally, the model reproduces the average
12 structure of the cloud system in 3P, but LWP and liquid COT are overestimated on the Western part
13 of the domain.

14 As shown in Table 4, R_e values averaged over the entire domain is underestimated by the model by
15 a factor of about 1.5 during all three periods of interest. LWP, values averaged over the entire
16 domain, is also overestimated in all three cases by a factor of 1.1, 1.3 and 1.6 for 1P, 2P, and 3P,
17 respectively. The R_e (LWP) underprediction (overestimation) may be due to the overestimation of
18 droplet number concentration that stems from overestimation of CN. Another reason that could
19 explain the positive bias of modelled LWP, is the inefficient autoconversion of cloud water to rain,
20 typical of the Morrison microphysical scheme (Saide et al., 2012). The consequence of the negative
21 (positive) of R_e (LWP) is the overestimation of average liquid COT by few percent for 1P and 3P,
22 and 42% for 2P.

23 The biases found here are quite different from the WRF/Chem study by Yang et al. (2011) on the
24 modelling of marine stratocumulus in Southeast Pacific. They have shown a bias of +30% in
25 reproducing the COT, while LWP was underestimated by a factor 1.3. The reader should note that
26 in Yang et al. (2011) the aerosol model adopted was different from the one used here and SOA
27 formation was not included at all.

28 Figure 13 displays the distribution functions (DF) of R_e , LWP and liquid COT for 1P. The DF for
29 2P and 3P are reported in the Supplement (Figure S6 and S7). In all three periods analysed, the
30 model captures the frequency of large droplets ($R_e > 18-20 \mu\text{m}$), underestimates the number of small
31 droplets ($8-10 < R_e < 18-20 \mu\text{m}$), and overestimates the frequency of very small cloud droplets ($R_e < 8-10 \mu\text{m}$) by more 30%. Whereas DF of the observed R_e presents the maximum in the range of 8-13 μm , modelled DF shows the maximum values in correspondence of the droplets with size less than

1 7-8 μm . WRF/Chem captures the shape of the distribution functions of LWP and liquid COT, but
2 underestimates the maximum and overestimates the higher and lower end of the distributions. Both
3 variables show a variability higher than the observations. The predicted standard deviations (Table
4 4) are about 2-3 and 1.5 times larger than those observed for LWP and liquid COT, respectively.
5 This probably stems from the large variability in simulated CCN.

6 Now it is interesting to analyse the model behaviour in reproducing the total CWP and COT given
7 by contribution of all cloud phases. Modelled CWP was calculated by vertically integrating all
8 cloud mixing ratio (water, rainwater, ice, snow and graupel). Predicted COT is given by the
9 contribution of the liquid water and ice. The contribution of the liquid water was calculated as
10 described above for liquid water cloud. The contribution of ice phase to COT was calculated
11 following Ebert and Curry (1992).

12 Figure 14 displays the comparison between observed and predicted CWP and COT in P1, whereas
13 the same figures for P2 and P3 are reported in the Supplement (Figures S8 and S9). Although for all
14 three cases, the model reproduces with good approximation the shape and localizations of the cloud
15 systems, CWP and COT are systematically overestimated (except COT in P2). As shown in Table
16 5, the predicted domain average of CWP presents, indeed, a bias of 62%, 41%, and 80% for P1, P2
17 and P3, respectively, whereas the bias of COT is about 15% in P1 and P3.

18 At this point of the analysis, although the aerosol-cloud interaction is a very complex nonlinear
19 process, we are able to relate the model error in aerosol particles to the uncertainties in cloud
20 prediction. The overestimation of CN leads to overprediction of the CCN. Higher number of CCN
21 means clouds with higher number of cloud droplets, higher water content, smaller droplets and
22 clouds optically deeper.

23 In addition to the uncertainties in aerosol particle simulation, one typical source of error in the
24 prediction of cloud fields, are the choices related to the model setup. For example Otkin and
25 Greenwald (2008) found a strong sensitivity of cloud properties while evaluating the response of
26 WRF model to the permutation of several PBL and cloud microphysical schemes. Moreover, the
27 same authors have shown that the low level clouds are sensitive to PBL parameterization, whereas
28 the upper level clouds are sensitive to both PBL and microphysics schemes.

29 One element that may affect the model-satellite comparison are the uncertainties associated to the
30 retrieval. For example, in South-Pacific stratocumulus, MODIS overestimates the droplet effective
31 radius by 13-20% with respect to concomitant in situ measurements (Painemal and Zuidema, 2011;
32 King et al., 2013). The overestimation of COT by MODIS results in the overestimation of CWP
33 (King et al., 2013). Henrich et al. (2010) have shown systematic differences between MODIS data

1 and in situ observations. Indeed, analysing a system of thin cumulus clouds during EUCAARI
2 campaign, they also found that MODIS overestimates the droplet effective radius by a factor 2-3
3 and COT is 2-3 times lower than in situ measurements.

4

1 **5 Impact of SOA particles on cloud prediction**

2 The last part of this study focused on the evaluation of the impact of SOA on the simulation of
3 cloud fields. We performed sensitivity simulations during P1, P2 and P3 without the SOA
4 (NOSOA), and compared them to the reference run (CTRL) discussed so far. NOSOA runs are
5 carried out only in the higher resolution domain (D3). The simulations of all three periods are
6 initialized at 00 UTC with the same meteorological and chemical input data used for CTRL, except
7 chemical initial conditions that are restarted by previous NOSOA run. Each period is preceded by
8 30 hours of simulation used as spin-up for D3 chemistry. The sensitivity simulation is performed
9 zeroing the arrays pertaining to SOA. Thus, the SOA fields are not affected by incoming SOA from
10 domain boundaries or by local production. We did not perform the sensitivity tests with SORGAM
11 option because this model produces very little SOA mass concentrations (Grell et al., 2005;
12 McKeen et al. 2007; Tuccella et al., 2012). Therefore, we may assume that simulations with
13 SORGAM and without SOA (in VBS option) are roughly equivalent. The advantage of this
14 assumption is that the model is forced with same initial meteorological conditions and boundary
15 meteorological and chemical conditions of the CTRL simulation. The use of SORGAM would
16 require to run the model on all three domains, leading to different results on D2 which is used to
17 initialize D3. Finally, this would introduce dependencies on the D3 input data making the
18 comparison not directly comparable to the CTRL run.

19 The comparisons of R_e , LWP and liquid COT simulated of CTRL and NOSOA runs with MODIS
20 data are reported in Figures 12, S4 and S5. In general, the average spatial pattern of these three
21 variables is captured better by CTRL simulation with respect to NOSOA run, especially in P1.
22 Figures 13, S6 and S7 display the comparison between DFs of the cloud properties simulated by
23 CTRL and NOSOA runs with those retrieved with MODIS observations. The domain averages for
24 each variable are reported in Table 4. NOSOA runs show a domain averaged R_e larger than CTRL.
25 DFs of the LWP are different between the runs, but it is not clear if there are improvements in
26 CTRL with respect to NOSOA run. Only the domain averages allow to establish that LWP values
27 predicted by CTRL run are closer to the observed means than NOSOA. The presence of SOA in the
28 numerical prediction improves the DF of liquid COT with respect to NOSOA simulation in P1 and
29 P3, whereas there are no differences during P2. NOSOA has 10% and 3% more optically thin liquid
30 clouds (liquid COT<40) with respect to CTRL in P1 and P3, respectively.

31 Figures 14, S8 and S9 report the comparison of modelled CWP and COT of all cloud phases predict
32 in CTRL and sensitivity runs with MODIS data. As well as for liquid phase, including SOA aerosol
33 particles in the runs, the WRF/Chem skills to reproduce the observed pattern of observed CWP and

1 COT increase. As shown in Table 5, domain averaged CWP and COT are larger up to about 50% in
2 CTRL with respect to NOSOA.

3 Now it is interesting to explore the impact of SOA on the vertical structure of the cloud fields. As
4 example we chose the 17 May because around 6 UTC, a frontal system associated to a trough from
5 North Sea crossed the Benelux area (Figure S10). In both runs, some isolated and shallow clouds
6 form during the night. When the cold front reaches Benelux around 5-6 UTC, a low pressure centre
7 forms (Figure S11). The winds rotate around the low pressure with speeds up to 14 m/s at 925 hPa
8 height (Figure S12). A convective system develops around the vortex. Figure 15 shows the
9 maximum radar reflectivity (maximum dBZ) at 6 UTC for CTRL simulation, and the difference of
10 maximum dBZ between CTRL and NOSOA runs. In general, the echo is larger for run with SOA,
11 i.e. the intensity of the storm is stronger in the CTRL run. Figures 16 and 17 show the vertical fields
12 of PM_{2.5} mass, vertical wind, liquid and frozen hydrometeor for both runs in the cross section A
13 displayed in Figure 15. These differences between both simulations (CTRL-NOSOA) along the
14 cross section A, are also displayed in Figures 16 and 17. The convection appears to be stronger in
15 the control simulation, with a larger amount of hydrometeors and stronger updrafts and downdrafts.
16 The larger differences in the simulated fields of vertical wind and hydrometeors occur in the same
17 location where occurs the enhancement of PM_{2.5} mass at cloud base (950-900 hPa), roughly at the
18 distance of 5-15 and 40-90 km away of the origin of the cross section A (Figures 16 and 17). The
19 results should be taken with caution because the aerosol-cloud interaction is treated only for liquid
20 clouds, the interaction of aerosol with ice phase is still missing in the model. Although the aerosol-
21 cloud interaction is a nonlinear process, it is possible to give an interpretation of the results with the
22 conceptual model for cloud invigoration proposed by Rosenfeld et al. (2008). The larger number of
23 CCN in CTRL may curb the autoconversion rate of droplets to raindrops, therefore the beginning of
24 precipitation may be delayed with respect to NOSOA. This delay leads to a larger amount of
25 condensed water that crosses the freezing level and forms ice hydrometeors. The freezing process
26 warms the higher layers of the cloud through release of latent heat, whereas the melting process due
27 to falling of ice cools the lower levels. This thermodynamic disequilibrium enhances the upward
28 transport of heat. The enhanced conversion of CAPE to kinetic energy may yield the cloud
29 invigoration found in the CTRL simulation.

6 Summary and conclusions

Secondary organic aerosol particles play an important role in the aerosol-cloud-radiation interaction because they contribute to the global budget of radiation and cloud condensation nuclei (CCN). The introduction of SOA particles in numerical simulations has the potential to reduce the uncertainties on the prediction of meteorological fields and air quality. To this aim, a parameterization for SOA production based on the recent VBS approach was coupled with microphysics and radiative schemes in the WRF/Chem community model.

The performance of the updated model at cloud resolving scale (2 km horizontal resolution) was evaluated using ground- and aircraft-based measurements collected during the IMPACT-EUCAARI campaign and the data from the MODIS satellite instrument. The study focuses on the Benelux area, around the supersite of Cabauw, from 14 to 30 May 2008. The analysed period was characterized by few days of high pressure (14-15 May), followed by a scavenged background situation (17-20 May), and finally by long range transport of Saharan dust with the passage of southerly fronts (23-31 May).

The model reproduces the variations of meteorological variables as a function of the synoptic frame. The model broadly captures the inter- and infra-diurnal variability of O_3 and NO_x at the surface. The concentration of NH_3 is underestimated. Concentrations of HNO_3 and $HONO$ is reproduced with poor correlation. Simulated SO_2 shows a positive bias of +90%, probably due to overestimated point sources. Surface aerosol mass of SO_4 , NO_3 , NH_4 , and OM is simulated with a correlation larger than 0.55. Their diurnal variations as a function of the synoptic frame are resolved by the model. The bias of simulated inorganic aerosol mass is explainable together with error of SO_2 , NH_3 , and HNO_3 in terms of anthropogenic emissions and the approximation to instantaneous thermodynamic equilibrium. The performances in reproducing the surface aerosol mass found here are comparable to other European studies where these variables are simulated with correlations range from 0.5-0.7 (e.g., Lecœur and Seigneur, 2013; Zhang et al., 2013b; Balzarini et al., 2014 for inorganic species; Athanasopoulou et al., 2013; Fountoukis et al. 2014; Li et al., 2013; Knote et al., 2011; for organic aerosols).

The analysis of aircraft data reveals that WRF/Chem captures the aerosol mass trend both in the PBL and the free troposphere (FT). The predicted aloft aerosol mass of each species is within the observed values range, but the model does not capture the full range of the measured concentrations: the modelled standard deviations of aerosol mass are lower than those observed. Nevertheless, SO_4 (NO_3 and NH_4) mass is overpredicted (underpredicted) in more than half of the flights. SO_4 bias is attributable to the SO_2 excess and to a potential overproduction within the cloud

1 chemistry scheme. The negative bias of NO_3 and NH_4 could be explained by a low concentration of
2 NH_3 that limits the formation of the ammonium-nitrate. The simulated OM concentration is at
3 lower end of the observed mass. The bias is attributable to the missing aqueous chemistry processes
4 of organic compounds, uncertainties in meteorological fields, to assumptions on the VBS approach
5 such as the SOA formation pathways, oxidation rate and dry deposition velocity of organic
6 condensable vapours. Another source of error in simulating SOA are the uncertainties in the
7 anthropogenic emissions of primary organic carbon and in the factor (1.6) used to convert them to
8 POM. In general, the statistical analysis reveals that the predicted average concentrations of
9 inorganic aerosols show absolute error of 2-8% in the PBL, while the NO_3 and NH_4 are simulated
10 with a bias of +14% and +20% (+0.3 and +0.2 $\mu\text{g}/\text{m}^3$), respectively, in the FT. The mean OM mass
11 is underestimated by a factor 2 and 3 in the PBL and FT, respectively. These biases are similar to
12 those reported by Fast et al. (2014) comparing WRF/Chem (but with a different chemistry package)
13 to aircraft data performed over California. Indeed they found an absolute mean bias of about 0.01-
14 0.2, 0.03-0.6, 0.1-0.45, 0.2-0.57 $\mu\text{g}/\text{m}^3$ for SO_4 , NO_3 , NH_4 , and OM, respectively. However, we
15 highlighted that the comparison of aerosol composition predicted by the model with AMS
16 measurements could be affected by a bias because the model concentrations are representative of
17 $\text{PM}_{2.5}$ particles and AMS collects aerosols with diameter only between 100-700 nm.

18 Condensation nuclei (CN) are overestimated by a factor of 1.4 and 1.7 in the PBL and FT,
19 respectively. However, in some cases, the predicted CN are overestimated by a factor of 3.
20 Predicted CN show higher variability than measurements. The model correlation with observed CN
21 is 0.40 and 0.74 in PBL and FT, respectively. These values are consistent with the 0.61 below 10
22 km of altitude found by Luo and Yu (2011) in the Eastern United States with WRF/Chem including
23 an advanced aerosol microphysical model. Model biases in predicting CN are attributable in large
24 part to the uncertainties of primary particle emissions (mostly in the PBL) and to the nucleation
25 rate.

26 The bias of simulated CCN is more contained with respect to that of CN. The CCN efficiency
27 (CCN/CN ratio) is underestimated by a factor of 1.5 and 3.8 in the PBL and FT, respectively. This
28 could be due to a low number of particles in the accumulation and coarse mode or to uncertainties
29 in the hygroscopicity of aerosol particles. CCN/CN ratio represents the ability of aerosol particles to
30 nucleate in cloud droplets. Therefore, its misrepresentation may lead to issues in the simulation of
31 cloud droplet number. In other words, the uncertainties in CCN efficiency is a general modelling
32 problem that may prevent a correct representation of the amplitude of the aerosol-cloud interaction,
33 i.e. the response of microphysical cloud properties to the variation of CCN **concentrations**. This

issue surely deserves and warrants further insight in the future, studies on the sensitive of the CCNs to emission distribution in the lognormal modes, aerosol hygroscopicity and updraft velocity are desirable to improve the aerosol activation in the models.

The bias of simulated CN affects the prediction of droplet effective radius (R_e), aerosol optical thickness (AOT), cloud water path (CWP), and cloud optical thickness (COT). The comparison with MODIS data shows that the model overestimates the AOT. The AOT averaged over the entire domain on a single day are 0.38 ± 0.12 and 0.42 ± 0.10 for MODIS and WRF/Chem data, respectively. The domain averaged R_e of liquid cloud droplets is underestimated by a factor of 1.5 in all the periods examined in the main text. Modelled mean cloud liquid water path (LWP) is also overestimated by a factor 1.1-1.6. The consequence of the negative (positive) bias of R_e (LWP) is the overestimation of average liquid COT by few percent up to 42%. CWP and COT of all cloud phases are systematically in 2 out of 3 periods analysed. Predicted domain average of CWP presents a bias that ranges from 41-80%, whereas the bias of COT is about 15% in P1 and P3. The overprediction of CWP could be due to the overestimation of droplet number concentration that results from the overestimation of CN, and to inefficient autoconversion of cloud water to rain. The reader should note that the model error found here are different from the study conducted with WRF/Chem by Yang et al. (2011) on the modelling of marine stratocumulus in Southeast Pacific where SOA formation was not included in the simulations. Those authors reported a bias of +30% in reproducing the COT, while CWP was underestimated by a factor 1.3.

In summary, the model behaviour of this new chemistry option in WRF/Chem in simulating the relationship between aerosol and cloud fields may be summarized by this way. The overestimation of CN results in the overprediction of the CCN. Higher number of CCN leads to clouds with higher number of cloud droplets, higher water content, smaller droplets and clouds optically deeper.

As test application of the new chemistry option, we performed a sensitivity simulation where SOA mass concentration is set to zero. The aim was to answer two questions:

1. Does the introduction of SOA particles improve the numerical prediction of cloud fields?

The introduction of SOA in the numerical simulations improves the predicted spatial pattern of microphysical and optical properties of cloud in liquid and all phases. NOSOA runs show an average R_e larger than CTRL. The analysis of LWP distribution function does not reveal a clear difference between CTRL and NOSOA simulations during the examined periods, only the domain averages allow to establish that LWP values predicted by CTRL run are closer to the observed means than NOSOA. Conversely, including SOA in the numerical prediction improves the distribution function of liquid COT with respect to NOSOA in 2 out

of 3 cases. In these two cases, NOSOA has up to 10% more optically thin liquid clouds (COT<40) with respect to CTRL. Finally, with regards to CWP and COT (all phase), including SOA aerosol particles in the runs, the WRF/Chem improves to reproduce the observed pattern of observed CWP and COT.

2. What is the impact of SOA particles on cloud development?

The analysis was conducted on a convective system. The simulated radar reflectivity is larger for run with SOA, i.e. the intensity of the storm is stronger in the CTRL run. The CTRL simulation exhibits a larger amount of hydrometeors and stronger updrafts and downdrafts. The larger differences in the simulated fields of vertical wind and hydrometeors are associated to the larger differences of PM_{2.5} mass located at the cloud base.

On the basis of the results discussed in this work, the option RACM/MADE/VBS coupled with cloud microphysics and radiation allows the WRF/Chem community to use a powerful tool for the study of the aerosol-cloud interactions, improved in terms of representation of the aerosol processes with respect to previous versions based on the RADM/MADE/SORGAM scheme.

For the future, there is still large space for improvements. For example, a more advanced treatment of deposition of organic condensable vapours is desirable. Moreover, the missing production of SOA in cloud is a gap that should also be filled. Finally, the extension of aerosol-cloud interaction to the ice-phase would lead to a complete representation of the aerosol indirect effects.

1 **Code availability**

2 The code updated, described, and evaluated here will be incorporated in the next available release
3 of WRF/Chem. The users will be able to freely download the code from the WRF website
4 (http://www2.mmm.ucar.edu/wrf/users/download/get_source.html). A general WRF/Chem user's
5 guide is also available online (<http://ruc.noaa.gov/wrf/WG11/>).

7 **Acknowledgements**

8 This work was founded by the University of L'Aquila (Italy) and Regione Abruzzo in the frame of
9 "High Formation Project" (P.O.F.S.E 2007-2013), and the Italian Space Agency in the frame of the
10 PRIMES (contract I/017/11/0) project. Paolo Tuccella is grateful to the National and Oceanic
11 Administration (NOAA) of Boulder (CO, USA) for the hospitality, to Ravan Ahmadov and Stuart
12 McKeen for the precious and profitable discussions about the parameterization for secondary
13 organic aerosol, and to Steven Peckham for the assistance in the implementation of the new
14 chemical option in the repository version of WRF/Chem. We are grateful to the Euro-Mediterranean
15 Center on Climate Change (CMCC) for having made available their supercomputer to perform the
16 numerical simulations. The authors thank Hugo Denier van der Gon for providing the TNO
17 emissions. Finally, the authors are grateful to two anonymous reviewers for their suggestions that
18 helped to improve this paper.

19

20

1 APPENDIX A: Technical details of coupling of VBS scheme with radiation and 2 microphysics schemes

3 The new chemistry option in namelist.input is *chem_opt=44*. It works with both *Lin* and *Morrison*
4 microphysics scheme, *Goddard* and *RRTM* shortwave scheme, and *RRTM* longwave
5 parameterization. Coupling of new scheme for SOA production with microphysics and radiative
6 processes requires several modifications to code:

- 7 1. The first step is to create a new chemistry option. The package *racm_soa_vbs_aqchem_kpp*
8 (*chemopt==44*) has been added to */Registry/registry.chem* together to some new model
9 variables for the cloud-borne organic aerosols, called, for example, *asoalcwi*, *asoalcwj* etc.
- 10 2. New chemistry package is a KPP option. Therefore, we created a new subdirectory in
11 */chem/KPP/mechanisms/racm_soa_vbs_aqchem* containing the files (*.spc, *.eqn, *.kpp,
12 and *.def) where are defined the chemical model species and constants, chemical reactions
13 in KPP format, model description, computer language, precision and integrator. The files are
14 the same used in *racm_soa_vbs_kpp* package (*chemopt==108*).
- 15 3. The last step is to update the subroutines in *chem* subdirectory. In order to call necessary
16 subroutines, the modules that we modified are:

- 17 • *chemics_init.F*
- 18 • *module_input_chem_data.F*
- 19 • *mechanism_driver.F*
- 20 • *cloudchem_driver.F*
- 21 • *module_sorgam_aqchem.F*
- 22 • *module_wetscav_driver.F*
- 23 • *module_aerosols_soa_vbs.F*
- 24 • *aerosol_driver.F*
- 25 • *dry_dep_driver.F*
- 26 • *module_mixactivate_wrappers.F*
- 27 • *emissions_driver.F*
- 28 • *module_bioemi_megan2.F*
- 29 • *optical_driver.F*
- 30 • *module_optical_averaging.F*
- 31 • *module_ctrans_grell.F*

1 APPENDIX B: Statistical indices used in the model evaluation

2 Let Obs_i and Mod_i be the observed and modeled values at time i , and N the number of
3 observations.

- 4 • The Pearson's Correlation (r):

$$5 \quad r = \frac{1}{N} \sum_{i=1}^N Z_i(Mod) \cdot Z_i(Obs)$$
$$6 \quad Z(X) = \frac{X - \langle X \rangle}{\sigma_X}$$

7 where X is a generic vector, $Z(X)$ is its standard score, and σ_X is the standard deviation.

- 8 • Mean Bias:

$$9 \quad MB = \frac{1}{N} \left(\sum_{i=1}^N Mod_i - Obs_i \right)$$

- 10 • Normalized Mean Bias (NMB):

$$11 \quad NMB = \frac{1}{N} \sum_{i=1}^N \frac{Mod_i - Obs_i}{Obs_i} \times 100$$

- 12 • Normalized Mean Gross Error (NMGE):

$$13 \quad NMGE = \frac{1}{N} \sum_{i=1}^N \frac{|Mod_i - Obs_i|}{Obs_i} \times 100$$

14

1 **References**

- 2 Aan de Brugh, J. M. J., Henzing, J. S., Schaap, M., Morgan, W. T., van Heerwaarden, C. C.,
3 Weijers, E. P., Coe, H., and Krol, M. C.: Modelling the partitioning of ammonium nitrate in the
4 convective boundary layer, *Atmos. Chem. Phys.*, 12, 3005-3023, doi:10.5194/acp-12-3005-2012,
5 2012.
- 6 Abdul-Razzak, H. and Ghan, S. J.: A parameterization of aerosol activation, 2, Multiple aerosol
7 types, *J. Geophys. Res.*, 105, 6837–6844, DOI: 10.1029/1999JD901161, 2000.
- 8 Abdul-Razzak, H. and Ghan, S. J.: A Parameterization of Aerosol Activation. 3. Sectional
9 Representation, *J. Geophys. Res.*, 107, 4026, doi:10.1029/2001JD000483, 2002.
- 10 Ackermann, I. J., Hass, H., Memmsheimer, M., Ebel, A., Binkowski, F. S., and Shankar, U.: Modal
11 aerosol dynamics model for Europe: development and first applications, *Atmos. Environ.*, 32 (17),
12 2981-2999, DOI: 10.1016/S1352-2310(98)00006-5, 1998.
- 13 Ahmadov, R., McKeen, S. A., Robinson, A., Bahreini, R., Middlebrook, A., de Gouw, J., Meagher, J.,
14 Hsie, E., Edgerton, E., Shaw, S., and Trainer, M.: A volatility basis set model for summertime
15 secondary organic aerosols over the eastern United States in 2006, *J. Geophys. Res.*, 117, D06301,
16 doi:10.1029/2011JD016831, 2012.
- 17 Andreae, M. O, and Rosenfeld, D.: Aerosol-cloud-precipitation interactions. Part 1. The nature and
18 sources of cloud-active aerosols, *Earth-Science Reviews*, 89, 13-41, DOI:
19 10.1016/j.earscirev.2008.03.001, 2008.
- 20 Asmi, E., Freney, E., Hervo, M., Picard, D., Rose, C., Colomb, A., and Sellegri, K.: Aerosol cloud
21 activation in summer and winter at puy-de-Dôme high altitude site in France, *Atmos. Chem. Phys.*,
22 12, 11589-11607, doi:10.5194/acp-12-11589-2012, 2012.
- 23 Athanasopoulou, E., Vogel, H., Vogel, B., Tsimpidi, A. P., Pandis, S. N., Knote, C., and
24 Fountoukis, C.: Modeling the meteorological and chemical effects of secondary organic aerosols
25 during an EUCAARI campaign, *Atmos. Chem. Phys.*, 13, 625-645, doi:10.5194/acp-13-625-2013,
26 2013.
- 27 Baklanov, A., Schlünzen, K., Suppan, P., Baldasano, J., Brunner, D., Aksoyoglu, S.,
28 Carmichael, G., Douros, J., Flemming, J., Forkel, R., Galmarini, S., Gauss, M., Grell, G., Hirtl, M.,
29 Joffre, S., Jorba, O., Kaas, E., Kaasik, M., Kallos, G., Kong, X., Korsholm, U., Kurganskiy, A.,
30 Kushta, J., Lohmann, U., Mahura, A., Manders-Groot, A., Maurizi, A., Moussiopoulos, N.,
31 Rao, S. T., Savage, N., Seigneur, C., Sokhi, R. S., Solazzo, E., Solomos, S., Sørensen, B.,

1 Tsegas, G., Vignati, E., Vogel, B., and Zhang, Y.: Online coupled regional meteorology chemistry
 2 models in Europe: current status and prospects, *Atmos. Chem. Phys.*, 14, 317-398, doi:10.5194/acp-
 3 14-317-2014, 2014.

4 Balzarini, A., Pirovano, G., Honzak, L., Zabkar, R., Curci, G., Forkel, R., Hirtl, M., San José, R.,
 5 Tuccella, P., and Grell, G. A.: WRF-Chem model sensitivity to chemical mechanism choice in
 6 reconstructing aerosol optical properties, *Atmos. Environ.*, doi:10.1016/j.atmosenv.2014.12.033,
 7 2014, in press.

8 Barnard, J. C., Fast, J. D., Paredes-Miranda, G., Arnott, W. P., and Laskin, A.: Technical Note:
 9 Evaluation of the WRF-Chem “Aerosol Chemical to Aerosol Optical Properties” Module using data
 10 from the MILAGRO campaign, *Atmos. Chem. Phys.*, 10, 7325–7340, doi:10.5194/acp-10-7325-
 11 2010, 2010.

12 Bao, J.-W., Michelson, S. A., McKeen, S. A., and Grell, G. A.: Meteorological evaluation of a
 13 weather-chemistry forecasting model using observations from the TEXAS AQS 2000 field
 14 experiment, *J. Geophys. Res.*, 110, D21105, doi:10.1029/2004JD005024, 2005.

15 Bègue, N., Tulet, P., Pelon, J., Aouizerats, B., Berger, A., and Schwarzenboeck, A.: Aerosol
 16 processing and CCN formation of an intense Saharan dust plume during the EUCAARI 2008
 17 campaign, *Atmos. Chem. Phys. Discuss.*, 14, 27039-27091, doi:10.5194/acpd-14-27039-2014,
 18 2014.

19 Bei, N., Li, G., and Molina, L. T.: Uncertainties in SOA simulations due to meteorological
 20 uncertainties in Mexico City during MILAGRO-2006 field campaign, *Atmos. Chem. Phys.*, 12,
 21 11295-11308, doi:10.5194/acp-12-11295-2012, 2012.

22 Bessagnet, B., Seigneur, C., and Menut, L.: Impact of dry deposition of semi-volatile organic
 23 compounds on secondary organic aerosols, *Atmos. Environ.*, 44, 1781-1787, DOI:
 24 10.1016/j.atmosenv.2010.01.027, 2010.

25 Boucher, O., Randall, D., Artaxo, P., Bretherton, C., Feingold, G., Forster, P., Kerminen, V.-M.,
 26 Kondo, Y., Liao, H., Lohmann, U., Rasch, P., Satheesh, S. K., Sherwood, S., Stevens B., and
 27 Zhang, X. Y.: Clouds and Aerosols. In: *Climate Change 2013: The Physical Science Basis*.
 28 Contribution of Working Group I to the Fifth Assessment Report of the Intergovernmental Panel on
 29 Climate Change [Stocker, T. F., D. Qin, G.-K. Plattner, M. Tignor, S. K. Allen, J. Boschung, A.
 30 Nauels, Y. Xia, V. Bex and P. M. Midgley (eds.)]. Cambridge University Press, Cambridge, United
 31 Kingdom and New York, NY, USA, , 2013.

1 Brunner, D., Jorba, O., Savage, N., Eder, B., Makar, P., Giordano, L., Badia, A., Balzarini, A.,
 2 Baro, R., Bianconi, R., Chemel, C., Forkel, R., Jimenez-Guerrero, P., Hirtl, M., Hodzic, A.,
 3 Honzak, L., Im, U., Knote, C., Kuenen, J. P. P., Makar, P. A., Manders-Groot, A., Neal, L., Perez,
 4 J. L., Pirovano, G., San Jose, R., Savage, N., Schroder, W., Sokhi, R. S., Syrakov, D., Torian, A.,
 5 Tuccella, P., Werhahn, K., Wolke, R., van Meijgaard, E., Yahya, K., Zabkar, R., Zhang, Y., Zhang,
 6 J., Hogrefe, C., Galmarini, S.: Evaluation of the meteorological performance of coupled chemistry-
 7 meteorology models in phase 2 of the air quality model evaluation international initiative, *Atmos.*
 8 *Environ.*, doi:10.1016/j.atmosenv.2014.12.032, 2014, in press.

9 Clarke, A., and Kapustin, A.: Hemispheric Aerosol Vertical Profiles: Anthropogenic Impacts on
 10 Optical Depth and Cloud Nuclei, *Science* 329, 1488, DOI: 10.1126/science.1188838, 2010.

11 Christensen, M. W., and Stephens, G. L.: Microphysical and macrophysical responses of marine
 12 stratocumulus polluted by underlying ships: Evidence of cloud deepening, *J. Geophys. Res.*, 116,
 13 D03201, doi:10.1029/2010JD014638, 2011.

14 Crumeyrolle, S., Schwarzenboeck, A., Roger, J. C., Sellegri, K., Burkhart, J. F., Stohl, A.,
 15 Gomes, L., Quennehen, B., Roberts, G., Weigel, R., Villani, P., Pichon, J. M., Bourrianne, T., and
 16 Laj, P.: Overview of aerosol properties associated with air masses sampled by the ATR-42 during
 17 the EUCAARI campaign (2008), *Atmos. Chem. Phys.*, 13, 4877-4893, doi:10.5194/acp-13-4877-
 18 2013, 2013.

19 Curci, G., Ferrero, L., Tuccella, P., Barnaba, F., Angelini, F., Bolzacchini, E., Carbone, C.,
 20 Denier van der Gon, H. A. C., Facchini, M. C., Gobbi, G. P., Kuenen, J. P. P., Landi, T. C.,
 21 Perrino, C., Perrone, M. G., Sangiorgi, G., and Stocchi, P.: How much is particulate matter near the
 22 ground influenced by upper level processes within and above the PBL? A summertime case study in
 23 Milan (Italy), *Atmos. Chem. Phys. Discuss.*, 14, 26403-26461, doi:10.5194/acpd-14-26403-2014,
 24 2014a.

25 Curci, G., Hogrefe, C., Bianconi, R., Im, U., Balzarini, A., Baro, R., Brunner, D., Forkel, R.,
 26 Giordano, L., Hirtl, M., Honzak, L., Jimenez-Guerrero, P., Knote, C., Langer, M., Makar, P.A.,
 27 Pirovano, G., Perez, J.L., San Jose, R., Syrakov, D., Tuccella, P., Werhahn, J., Wolke, R., Zabkar,
 28 R., Zhang, J., Galmarini, S.: Uncertainties of simulated aerosol optical properties induced by
 29 assumptions on aerosol physical and chemical properties: an AQMEII-2 perspective, *Atmos.*
 30 *Environ.*, doi: 10.1016/j.atmosenv.2014.09.009, 2014b, in press.

1 Easter, R. C., Ghan, S. J., Zhang, Y., Saylor, R. D., Chapman, E. G., Laulainen, N. S., Abdul-
2 Razzak, H., Leung, L. R., Bian, X., and Zaveri, R. A.: MIRAGE: Model Description and Evaluation
3 of Aerosols and Trace Gases, *J. Geophys. Res.*, 109, D20210, doi:10.1029/2004JD004571, 2004.

4 Ebert, E. E., and Curry, J. A.: A parameterization of ice cloud optical properties for climate models,
5 *J. Geophys. Res.*, 97, 3831-3836, DOI: 10.1029/91JD02472, 1992.

6 Elleman, R. A., Covert, D. S.: Aerosol size distribution modeling with the Community Multiscale
7 Air Quality modeling system in the Pacific Northwest: 3. Size distribution of particles emitted into
8 a mesoscale model, *J. Geophys. Res.*, 115, D03204, doi:10.1029/2009JD012401, 2010.

9 Emmons, L. K., Walters, S., Hess, P. G., Lamarque, J.-F., Pfister, G. G., Fillmore, D., Granier, C.,
10 Guenther, A., Kinnison, D., Laepple, T., Orlando, J., Tie, X., Tyndall, G., Wiedinmyer, C.,
11 Baughcum, S. L., and Kloster, S.: Description and evaluation of the Model for Ozone and Related
12 chemical Tracers, version 4 (MOZART-4), *Geosci. Model Dev.*, 3, 43–67, doi:10.5194/gmd-3-43-
13 2010, 2010.

14 Ervens, B., Turpin, B. J., and Weber, R. J.: Secondary organic aerosol formation in cloud droplets
15 and aqueous particles (aqSOA): a review of laboratory, field and model studies, *Atmos. Chem.*
16 *Phys.*, 11, 11069-11102, doi:10.5194/acp-11-11069-2011, 2011.

17 Fast, J. D., Allan, J., Bahreini, R., Craven, J., Emmons, L., Ferrare, R., Hayes, P. L., Hodzic, A.,
18 Holloway, J., Hostetler, C., Jimenez, J. L., Jonsson, H., Liu, S., Liu, Y., Metcalf, A.,
19 Middlebrook, A., Nowak, J., Pekour, M., Perring, A., Russell, L., Sedlacek, A., Seinfeld, J.,
20 Setyan, A., Shilling, J., Shrivastava, M., Springston, S., Song, C., Subramanian, R., Taylor, J. W.,
21 Vinoj, V., Yang, Q., Zaveri, R. A., and Zhang, Q.: Modeling regional aerosol and aerosol precursor
22 variability over California and its sensitivity to emissions and long-range transport during the 2010
23 CalNex and CARES campaigns, *Atmos. Chem. Phys.*, 14, 10013-10060, doi:10.5194/acp-14-
24 10013-2014, 2014.

25 Fountoukis, C., Megaritis, A. G., Skyllakou, K., Charalampidis, P. E., Pilinis, C.,
26 Denier van der Gon, H. A. C., Crippa, M., Canonaco, F., Mohr, C., Prévôt, A. S. H., Allan, J. D.,
27 Poulain, L., Petäjä, T., Tiitta, P., Carbone, S., Kiendler-Scharr, A., Nemitz, E., O'Dowd, C.,
28 Swietlicki, E., and Pandis, S. N.: Organic aerosol concentration and composition over Europe:
29 insights from comparison of regional model predictions with aerosol mass spectrometer factor
30 analysis, *Atmos. Chem. Phys.*, 14, 9061-9076, doi:10.5194/acp-14-9061-2014, 2014.

31 Ghan, S. J., Leung, L. R., Easter, R. C. and Abdul-Razzak, H.: Pre-diction of Droplet Number in a
32 General Circulation Model, *J. Geophys. Res.*, 102, 21777–21794, DOI: 10.1029/97JD01810, 1997.

1 Grell, G. A., Peckham, S. E., McKeen, S., Schmitz, R., Frost, G., Skamarock, W. C., and Eder, B.:
 2 Fully coupled “online” chemistry within the WRF model, *Atmos. Environ.*, 39, 6957–6975,
 3 doi:10.1016/j.atmosenv.2005.04.027, 2005.

4 Guenther, A., Karl, T., Harley, P., Wiedinmyer, C., Palmer, P. I., and Geron, C.: Estimates of global
 5 terrestrial isoprene emissions using MEGAN (Model of Emissions of Gases and Aerosols from
 6 Nature), *Atmos. Chem. Phys.*, 6, 3181-3210, doi:10.5194/acp-6-3181-2006, 2006.

7 Luo, G. and Yu, F.: Simulation of particle formation and number concentration over the Eastern
 8 United States with the WRF-Chem + APM model, *Atmos. Chem. Phys.*, 11, 11521-11533,
 9 doi:10.5194/acp-11-11521-2011, 2011.

10 Hallquist, M., Wenger, J. C., Baltensperger, U., Rudich, Y., Simpson, D., Claeys, M., Dommen, J.,
 11 Donahue, N. M., George, C., Goldstein, A. H., Hamilton, J. F., Herrmann, H., Hoffmann, T.,
 12 Iinuma, Y., Jang, M., Jenkin, M. E., Jimenez, J. L., Kiendler-Scharr, A., Maenhaut, W.,
 13 McFiggans, G., Mentel, Th. F., Monod, A., Prévôt, A. S. H., Seinfeld, J. H., Surratt, J. D.,
 14 Szmigielski, R., and Wildt, J.: The formation, properties and impact of secondary organic aerosol:
 15 current and emerging issues, *Atmos. Chem. Phys.*, 9, 5155-5236, doi:10.5194/acp-9-5155-2009,
 16 2009.

17 Haywood J., and Boucher O.: Estimates of the direct and indirect aerosol radiative forcing due to
 18 tropospheric aerosols: a review, *Reviews of Geophysics*, 38, 513–543,
 19 DOI: 10.1029/1999RG000078, 2000.

20 Hamburger, T., McMeeking, G., Minikin, A., Birmili, W., Dall'Osto, M., O'Dowd, C., Flentje, H.,
 21 Henzing, B., Junninen, H., Kristensson, A., de Leeuw, G., Stohl, A., Burkhardt, J. F., Coe, H.,
 22 Krejci, R., and Petzold, A.: Overview of the synoptic and pollution situation over Europe during the
 23 EUCAARI-LONGREX field campaign, *Atmos. Chem. Phys.*, 11, 1065-1082, doi:10.5194/acp-11-
 24 1065-2011, 2011.

25 Hansen, J., Sato, M., and Ruedy, R.: Radiative forcing and climate response, *J. Geophys. Res.*, 102,
 26 6831-6894, DOI: 10.1029/96JD03436 ,1997.

27 Henrich, F., Siebert, H., Jakel, E., Shaw, R. A., and Wendisch, M.: Collocated measurements of
 28 boundary layer cloud microphysical and radiative properties: a feasibility study, *J. Geophys. Res.*,
 29 115, D24214, doi:10.1029/2010JD013930, 2010.

30 Holt, T. R., Niyogi, D., Chen, F., Manning, K., LeMone, M., A., and Qureshi, A.: Effect of Land–
 31 Atmosphere Interactions on the IHOP 24–25 May 2002 Convection Case, *Monthly Weather*
 32 *Review*, 134, 113-133, doi: 10.1175/MWR3057.1, 2006.

1 Im, U., Bianconi, R., Solazzo, E., Kioutsioukis, I., Badia, A., Balzarini, A., Baro, R., Bellasio, R.,
2 Brunner, D., Chemel, C., Curci, G., Denier van der Gon, H., Flemming, J., Forkel, R., Giordano, L.,
3 Jimenez-Guerrero, P., Hirtl, M., Hodzic, A., Honzak, L., Jorba, O., Knote, C., Makar, P. A.,
4 Manders-Groot, A., Neal, L., Perez, J. L., Pirovano, G., Pouliot, G., San Jose, R., Savage, N.,
5 Schroder, W., Sokhi, R. S., Syrakov, D., Torian, A., Tuccella, P., Wang, K., Werhahn, J., Wolke,
6 R., Zabkar, R., Zhang, Y., Zhang, J., Hogrefe, C., and Galmarini, S.: Evaluation of operational
7 online-coupled regional air quality models over Europe and North America in the context of
8 AQMEII phase 2. Part II: Particulate Matter, *Atmos. Environ.*, doi:
9 10.1016/j.atmosenv.2014.08.072, 2014, in press.

10 King, N. J., Bower, K. N., Crosier, J., and Crawford, I.: Evaluating MODIS cloud retrievals with in
11 situ observations from VOCALS-REx, *Atmos. Chem. Phys.*, 13, 191-209, doi:10.5194/acp-13-191-
12 2013, 2013.

13 Knote, C., Brunner, D., Vogel, H., Allan, J., Asmi, A., Äijälä, M., Carbone, S., van der Gon, H. D.,
14 Jimenez, J. L., Kiendler-Scharr, A., Mohr, C., Poulain, L., Prévôt, A. S. H., Swietlicki, E., and
15 Vogel, B.: Towards an online-coupled chemistry-climate model: evaluation of trace gases and
16 aerosols in COSMO-ART, *Geosci. Model Dev.*, 4, 1077-1102, doi:10.5194/gmd-4-1077-2011,
17 2011.

18 Knote, C., Tuccella, P., Curci, G., Emmons, L., Orlando, J. J., Madronich, S., Barò, R., Jimenez-
19 Guerrero, P., Luecken, D., Hogrefe, C., Forkel, R., Werhahn, J., Hirtl, M., Pirez, J. L., San José,
20 R., Giordano, L., Brunner, D., Yahya, K., and Zhang, Y.: Influence of the choice of gas-phase
21 mechanism on predictions of key gaseous pollutants during the AQMEII phase-2 intercomparison,
22 *Atmos. Environ.*, doi:10.1016/j.atmosenv.2014.11.066, 2014a, in press.

23 Knote, C., Hodzic, A., and Jimenez, J. L.: The effect of dry and wet deposition of condensable
24 vapors on secondary organic aerosols concentrations over the continental US, *Atmos. Chem. Phys.*,
25 15, 1-18, doi:10.5194/acp-15-1-2015, 2015.

26 Koren, I., Altaratz, O., Remer, L. A., Feingold, G., Martins, J. V., and Heiblum, R. H.: Aerosol-
27 induced intensification of rain from the tropics to the mid-latitudes, *Nature Geoscience*, 5, 118-122,
28 doi:10.1038/ngeo1364, 2012.

29 Kuenen, J. J. P., Visschedijk, A. J. H., Jozwicka, M., and Denier van der Gon, H. A. C.: TNO-
30 MACC_II emission inventory; a multi-year (2003–2009) consistent high-resolution European
31 emission inventory for air quality modelling, *Atmos. Chem. Phys.*, 14, 10963-10976,
32 doi:10.5194/acp-14-10963-2014, 2014.

1 Kulmala, M., Asmi, A., Lappalainen, H. K., Baltensperger, U., Brenguier, J.-L., Facchini, M. C.,
 2 Hansson, H.-C., Hov, Ø., O'Dowd, C. D., Pöschl, U., Wiedensohler, A., Boers, R., Boucher, O.,
 3 de Leeuw, G., Denier van der Gon, H. A. C., Feichter, J., Krejci, R., Laj, P., Lihavainen, H.,
 4 Lohmann, U., McFiggans, G., Mentel, T., Pilinis, C., Riipinen, I., Schulz, M., Stohl, A.,
 5 Swietlicki, E., Vignati, E., Alves, C., Amann, M., Ammann, M., Arabas, S., Artaxo, P., Baars, H.,
 6 Beddows, D. C. S., Bergström, R., Beukes, J. P., Bilde, M., Burkhardt, J. F., Canonaco, F.,
 7 Clegg, S. L., Coe, H., Crumeyrolle, S., D'Anna, B., Decesari, S., Gilardoni, S., Fischer, M.,
 8 Fjaeraa, A. M., Fountoukis, C., George, C., Gomes, L., Halloran, P., Hamburger, T.,
 9 Harrison, R. M., Herrmann, H., Hoffmann, T., Hoose, C., Hu, M., Hyvärinen, A., Hörrak, U.,
 10 Iinuma, Y., Iversen, T., Josipovic, M., Kanakidou, M., Kiendler-Scharr, A., Kirkevåg, A., Kiss, G.,
 11 Klimont, Z., Kolmonen, P., Komppula, M., Kristjánsson, J.-E., Laakso, L., Laaksonen, A.,
 12 Labonnote, L., Lanz, V. A., Lehtinen, K. E. J., Rizzo, L. V., Makkonen, R., Manninen, H. E.,
 13 McMeeking, G., Merikanto, J., Minikin, A., Mirme, S., Morgan, W. T., Nemitz, E., O'Donnell, D.,
 14 Panwar, T. S., Pawlowska, H., Petzold, A., Pienaar, J. J., Pio, C., Plass-Duelmer, C.,
 15 Prévôt, A. S. H., Pryor, S., Reddington, C. L., Roberts, G., Rosenfeld, D., Schwarz, J., Seland, Ø.,
 16 Sellegri, K., Shen, X. J., Shiraiwa, M., Siebert, H., Sierau, B., Simpson, D., Sun, J. Y., Topping, D.,
 17 Tunved, P., Vaattovaara, P., Vakkari, V., Veefkind, J. P., Visschedijk, A., Vuollekoski, H.,
 18 Vuolo, R., Wehner, B., Wildt, J., Woodward, S., Worsnop, D. R., van Zadelhoff, G.-J.,
 19 Zardini, A. A., Zhang, K., van Zyl, P. G., Kerminen, V.-M., Carslaw, K., and Pandis, S. N.:
 20 General overview: European Integrated project on Aerosol Cloud Climate and Air Quality
 21 interactions (EUCAARI) – integrating aerosol research from nano to global scales, *Atmos. Chem.*
 22 *Phys.*, 11, 13061-13143, doi:10.5194/acp-11-13061-2011, 2011.

23 Lecœur, È. and Seigneur, C.: Dynamic evaluation of a multi-year model simulation of particulate
 24 matter concentrations over Europe, *Atmos. Chem. Phys.*, 13, 4319-4337, doi:10.5194/acp-13-4319-
 25 2013, 2013.

26 Lee, L. A., Pringle, K. J., Reddington, C. L., Mann, G. W., Stier, P., Spracklen, D. V., Pierce, J. R.,
 27 and Carslaw, K. S.: The magnitude and causes of uncertainty in global model simulations of cloud
 28 condensation nuclei, *Atmos. Chem. Phys.*, 13, 8879-8914, doi:10.5194/acp-13-8879-2013, 2013.

29 Li, Z., Niu, F., Fan, J., Liu, Y., Rosenfeld, D., and Ding, D.: Long-term impacts of aerosols on the
 30 vertical development of clouds and precipitation, *Nature Geoscience*, 4, 888-894,
 31 doi:10.1038/ngeo1313, 2011.

32 Li, Y. P., Elbern, H., Lu, K. D., Friese, E., Kiendler-Scharr, A., Mentel, Th. F., Wang, X. S.,
 33 Wahner, A., and Zhang, Y. H.: Updated aerosol module and its application to simulate secondary

1 organic aerosols during IMPACT campaign May 2008, *Atmos. Chem. Phys.*, 13, 6289-6304,
2 doi:10.5194/acp-13-6289-2013, 2013.

3 Li, X., Rohrer, F., Hofzumahaus, A., Brauers, T., Häseler, R., Bohn, B., Broch, S., Fuchs, H.,
4 Gomm, S., Holland, F., Jäger, J., Kaiser, J., Keutsch, F. N., Lohse, I., Lu, K., Tillmann, R.,
5 Wegener, R., Wolfe, G. M., Mentel, F. M., Kiendler-Scharr, A., and Wahner, A.: Missing Gas-
6 Phase Source of HONO Inferred from Zeppelin Measurements in the Troposphere, *Science*, 344,
7 292-296, DOI: 10.1126/science.1248999, 2014.

8 Lohmann, H., and Feichter, J.: Global indirect effects: a review, *Atmos. Chem. Phys.*, 5, 715-737,
9 doi:10.5194/acp-5-715-2005, 2005.

10 Yu, S., Mathur, R., Pleim, J., Wong, D., Gilliam, R., Alapaty, K., Zhao, C., and Liu, X.: Aerosol
11 indirect effect on the grid-scale clouds in the two-way coupled WRF-CMAQ: model description,
12 development, evaluation and regional analysis, *Atmos. Chem. Phys.*, 14, 11247-11285,
13 doi:10.5194/acp-14-11247-2014, 2014.

14 Meng, Z., Dabdud, D., and Seinfeld, J. H.: Chemical coupling between atmospheric ozone and
15 particulate matter, *Science*, 277, 116–119, doi:10.1126/science.277.5322.116, 1997.

16 Mensah, A. A., Holzinger, R., Otjes, R., Trimborn, A., Mentel, Th. F., ten Brink, H., Henzing, B.,
17 and Kiendler-Scharr, A.: Aerosol chemical composition at Cabauw, The Netherlands as observed in
18 two intensive periods in May 2008 and March 2009, *Atmos. Chem. Phys.*, 12, 4723-4742,
19 doi:10.5194/acp-12-4723-2012, 2012.

20 Merikanto, J., Spracklen, D. V., Mann, G. W., Pickering, S. J., and Carslaw, K. S.: Impact of
21 nucleation on global CCN, *Atmos. Chem. Phys.*, 9, 8601-8616, doi:10.5194/acp-9-8601-2009,
22 2009.

23 Misenis, C., and Zhang, Y. : An examination of sensitivity of WRF/Chem predictions to physical
24 parameterizations, horizontal grid spacing, and nesting options, *Atmos. Res.*, 97, 315-334, DOI:
25 10.1016/j.atmosres.2010.04.005, 2010.

26 McKeen, S., Chung, S. H., Wilczak, J., Grell, G., Djalalova, I., Peckham, S., Gong, W., Bouchet,
27 V., Moffet, R., Tang, Y., Carmichael, G. R., Mathur, R., and Yu, S.: Evaluation of several PM_{2.5}
28 forecast models using data collected during the ICARTT/NEAQS 2004 field study, *J. Geophys.*
29 *Res.*, 112, D10S20, doi:10.1029/2006JD007608, 2007.

1 Ngan, F., Kim, H., Lee, P., Al-Wali, K., and Dornblaser, B.: A Study of Nocturnal Surface Wind
 2 Speed Overprediction by the WRF-ARW Model in Southeastern Texas. *J. Appl. Meteor.*
 3 *Climatol.*, 52, 2638–2653, doi: 10.1175/JAMC-D-13-060.1, 2013.

4 O'Donnell, D., Tsigaridis, K., and Feichter, J.: Estimating the direct and indirect effects of
 5 secondary organic aerosols using ECHAM5-HAM, *Atmos. Chem. Phys.*, 11, 8635-8659,
 6 doi:10.5194/acp-11-8635-2011, 2011.

7 Otkin, J. A., and Greenwald, T. J.: Comparison of WRF model-simulated and MODIS-derived
 8 cloud data, *Mon. Wea. Rev.*, 136, 1957-1970, DOI:10.1175/2007MWR2293.1, 2008.

9 Painemal, D., and Zuidema, P.: Assessment of MODIS cloud effective radius and optical thickness
 10 retrievals over the Southeast Pacific with VOCALS-REx in situ measurements, *J. Geophys. Res.*,
 11 116, D24206, doi:10.1029/ 2011JD016155, 2011.

12 Pielke, R. A.: Influence of the spatial distribution of vegetation and soils on the prediction of
 13 cumulus convective rainfall, *Reviews of Geophysics*, 39, 2, DOI: 10.1029/1999RG000072, 2001.

14 Pierce, J. R. and Adams, P. J.: Uncertainty in global CCN concentrations from uncertain aerosol
 15 nucleation and primary emission rates, *Atmos. Chem. Phys.*, 9, 1339-1356, doi:10.5194/acp-9-
 16 1339-2009, 2009.

17 Roelofs, G.-J., ten Brink, H., Kiendler-Scharr, A., de Leeuw, G., Mensah, A., Minikin, A., and
 18 Otjes, R.: Evaluation of simulated aerosol properties with the aerosol-climate model ECHAM5-
 19 HAM using observations from the IMPACT field campaign, *Atmos. Chem. Phys.*, 10, 7709-7722,
 20 doi:10.5194/acp-10-7709-2010, 2010.

21 Rosenfeld, D., Lohmann, U., Raga, G. B., O'Dowd, C. D., Kulmala, M., Fuzzi, S., Reissel, A., and
 22 Andreae, M. O.: Flood or Drought: How do aerosols affect precipitation?, *Science*, 321, 1308-1313,
 23 DOI:10.1126/science.1160606, 2008.

24 Saide, P. E., Spak, S. N., Carmichael, G. R., Mena-Carrasco, M. A., Yang, Q., Howell, S.,
 25 Leon, D. C., Snider, J. R., Bandy, A. R., Collett, J. L., Benedict, K. B., de Szoeke, S. P.,
 26 Hawkins, L. N., Allen, G., Crawford, I., Crosier, J., and Springston, S. R.: Evaluating WRF-Chem
 27 aerosol indirect effects in Southeast Pacific marine stratocumulus during VOCALS-REx, *Atmos.*
 28 *Chem. Phys.*, 12, 3045-3064, doi:10.5194/acp-12-3045-2012, 2012.

29 Schell, B., Ackermann, I. J., Hass, H., Binkowski, F. S., and Ebel, A.: Modeling the formation of
 30 secondary organic aerosol within a comprehensive air quality model system, *J. Geophys. Res.*, 106,
 31 28275-28293, DOI: 10.1029/2001JD000384, 2001.

1 Scott, C. E., Rap, A., Spracklen, D. V., Forster, P. M., Carslaw, K. S., Mann, G. W., Pringle, K. J.,
2 Kivekäs, N., Kulmala, M., Lihavainen, H., and Tunved, P.: The direct and indirect radiative effects
3 of biogenic secondary organic aerosol, *Atmos. Chem. Phys.*, 14, 447-470, doi:10.5194/acp-14-447-
4 2014, 2014.

5 Sotiropoulou, R. E. P., Tagaris, E., Pilinis, C., Anttila, T., and Kulmala, M.: Modeling new particle
6 formation during air pollution episodes: Impacts on aerosol and cloud condensation nuclei, *Aerosol*
7 *Sci. Technol.*, 40, 557–572, doi:10.1080/02786820600714346, 2006.

8 Spracklen, D. V., Carslaw, K. S., Kulmala, M., Kerminen, V.-M., Mann, G. W., and Sihto, S.-L.:
9 The contribution of boundary Mann, G. W., and Sihto, S.-L.: The contribution of boundary gional
10 and global scales, *Atmos. Chem. Phys.*, 6, 5631–5648, doi:10.5194/acp-6-5631-2006, 2006.

11 Stern, R., Builtjes, P., Shaap, M., Timmermans, R., Vautard, R., Hodzic, A., Memmesheimer, M.,
12 Feldmann, H., Renner, E., Wolke, R., and Kershbaumer, A.: A model inter-comparison study
13 focussing on episode with elevated PM10 concentrations, *Atmos. Environ.*, 42, 4567-4588,
14 doi:10.1016/j.atmosenv.2008.01.068, 2008.

15 Stockwell, W. R., Middleton, P., Chang, J. S., and Tang, X.: The second-generation regional acid
16 deposition model chemical mechanism for regional air quality modeling, *J. Geophys. Res.*, 95,
17 16343-16367, DOI: 10.1029/JD095iD10p16343, 1990.

18 Ten Hoeve, J. E., Remer, L. A., and Jacobson, M. Z.: Microphysical and radiative effects of
19 aerosols on warm clouds during the Amazon biomass burning season as observed by MODIS:
20 impacts of water vapor and land cover, *Atmos. Chem. Phys.*, 11, 3021-3036, doi:10.5194/acp-11-
21 3021-2011, 2011.

22 Tuccella, P., Curci, G., Visconti, G., Bessagnet, B., Menut, L., and Park, R. J.: Modeling of gas and
23 aerosol with WRF/Chem over Europe: Evaluation and sensitivity study, *J. Geophys. Res.*, 117,
24 D03303, doi:10.1029/2011JD016302, 2012.

25 Turpin, B. J., and Lim, H.-J. : Species contributions to PM_{2.5} mass concentrations: Revisiting
26 common assumptions for estimating organic mass, *Aerosol Sci. Technol.*, 35, 602–610,
27 DOI: 10.1080/02786820152051454, 2001.

28 Walcek, C. J. and Taylor, G. R.: A theoretical method for computing vertical distributions of acidity
29 and sulfate production within cumulus clouds, *J. Atmos. Sci.*, 43, 339-355,
30 doi: [http://dx.doi.org/10.1175/1520-0469\(1986\)043<0339:ATMFCV>2.0.CO;2](http://dx.doi.org/10.1175/1520-0469(1986)043<0339:ATMFCV>2.0.CO;2), 1986.

1 Yang, Q., W. I. Gustafson Jr., Fast, J. D., Wang, H., Easter, R. C., Morrison, H., Lee, Y.-N.,
2 Chapman, E. G., Spak, S. N., and Mena-Carrasco, M. A.: Assessing regional scale predictions of
3 aerosols, marine stratocumulus, and their interactions during VOCALS-REx using WRF-Chem,
4 *Atmos. Chem. Phys.*, 11, 11951-11975, doi:10.5194/acp-11-11951-2011, 2011.

5 Zhao, C., Liu, X., Leung, L. R., Johnson, B., McFarlane, S. A., Gustafson Jr., W. I., Fast, J. D., and
6 Easter, R.: The spatial distribution of mineral dust and its shortwave radiative forcing over North
7 Africa: modeling sensitivities to dust emissions and aerosol size treatments, *Atmos. Chem. Phys.*,
8 10, 8821-8838, doi:10.5194/acp-10-8821-2010, 2010. Zhang, Y.: Online-coupled meteorology and
9 chemistry models: history, current status, and outlook, *Atmos. Chem. Phys.*, 8, 2895-2932,
10 doi:10.5194/acp-8-2895-2008, 2008.

11 Zhang, Y., Sartelet, K., Wu, S.-Y., and Seigneur, C.: Application of WRF/Chem-MADRID and
12 WRF/Polyphemus in Europe – Part 1: Model description, evaluation of meteorological predictions,
13 and aerosol–meteorology interactions, *Atmos. Chem. Phys.*, 13, 6807-6843, doi:10.5194/acp-13-
14 6807-2013, 2013a.

15 Zhang, Y., Sartelet, K., Zhu, S., Wang, W., Wu, S.-Y., Zhang, X., Wang, K., Tran, P., Seigneur, C.,
16 and Wang, Z.-F.: Application of WRF/Chem-MADRID and WRF/Polyphemus in Europe – Part 2:
17 Evaluation of chemical concentrations and sensitivity simulations, *Atmos. Chem. Phys.*, 13, 6845-
18 6875, doi:10.5194/acp-13-6845-2013, 2013b.

19

1

2 **TABLES**

3 Table 1. Physical and chemical parameterizations used in the simulation

Physical Processes	WRF/Chem parameterizations
Cloud Microphysics	Morrison
Cumulus Cloud	New Grell (D1 and D2)
Longwave radiation	RRTM
Shortwave radiation	RRTM
PBL	MYNN
Surface Layer	Monin-Obukov
Surface	Noah LSM
Gas-phase Chemistry	Modified RACM-ESRL
Aerosol Chemistry	MADE/SOA-VBS
Biogenic Emissions	MEGAN

4

5

1

2 Table 2. Statistical indices of the comparison of WRF/Chem to observations of temperature (T),
 3 relative humidity (RH), wind speed (WS), wind direction (WD), ozone (O₃), nitrogen oxide (NO_x),
 4 nitric dioxide (NO₂), nitric oxide (NO), ammonia (NH₃), nitric acid (HNO₃), nitrous acid (HONO),
 5 sulphur dioxide (SO₂), particle sulphate (SO₄), particle nitrate (NO₃), particle (ammonium), and
 6 particle OM, collected at Cabauw tower.

Variable	R	MB	NMB	NMGE
T (°C) at 2m	0.93	-0.66	-5.46	10.65
T (°C) at 10m	0.93	-0.67	-5.24	9.31
T (°C) at 20m	0.94	-0.56	-4.15	8.16
T (°C) at 40m	0.94	-0.46	-3.24	7.21
T (°C) at 80m	0.95	-0.32	-2.10	5.97
T (°C) at 140m	0.95	-0.26	-1.51	5.92
T (°C) at 200m	0.95	-0.45	-2.79	6.66
RH (%) at 2m	0.87	3.17	6.42	11.23
RH (%) at 10m	0.89	4.44	8.36	11.48
RH (%) at 20m	0.91	3.04	6.33	10.50
RH (%) at 40m	0.92	2.99	6.40	10.51
RH (%) at 80m	0.73	-1.04	2.13	13.34
RH (%) at 140m	0.92	2.81	6.40	11.19
RH (%) at 200m	0.91	2.99	7.44	12.50
WS (m/s) at 10m	0.78	0.67	27.90	35.56
WS (m/s) at 20m	0.66	1.27	40.89	49.32
WS (m/s) at 40m	0.67	1.26	32.64	42.04
WS (m/s) at 60m	0.72	1.23	24.42	38.99
WS (m/s) at 140m	0.74	1.21	28.66	41.55
WS (m/s) at 200m	0.76	1.13	27.79	41.48
WD (deg) at 10m	0.52	27.32	43.31	43.31
WD (deg) at 20m	0.53	24.80	40.48	40.48

WD (deg) at 40m	0.60	23.59	40.34	40.34
WD (deg) at 80m	0.67	20.22	30.34	30.34
WD (deg) at 140m	0.71	19.21	32.01	32.01
WS (deg) at 200m	0.73	17.18	28.46	28.46
<hr/>				
O ₃ (µg/m ³)	0.72	-3.43	70.03	90.88
NO _x (µg/m ³)	0.70	0.43	19.76	44.77
NO (µg/m ³)	0.65	0.28	116.08	167.59
NO ₂ (µg/m ³)	0.66	1.25	28.68	54.20
NH ₃ (µg/m ³)	0.43	-4.75	-27.72	42.94
HNO ₃ (µg/m ³)	0.21	-0.09	-1.22	108.65
HONO (µg/m ³)	0.05	-0.56	-95.37	95.37
SO ₂ (µg/m ³)	0.48	0.68	90.20	116.33
<hr/>				
SO ₄ (µg/m ³)	0.56	1.04	92.2	95.4
NO ₃ (µg/m ³)	0.68	1.00	72.4	94.3
NH ₄ (µg/m ³)	0.74	0.66	63.0	67.3
OM (µg/m ³)	0.75	-0.42	3.21	29.9

1

2

1

2 Table 3. Observed and modelled mean values, standard deviations, and relative amount (expressed
 3 as percentage) of aerosol species, number of aerosol particles, cloud condensation nuclei, over the
 4 whole period of the aircraft campaign in boundary layer and free troposphere.

	Boundary Layer			Free Troposphere		
	Observation	WRF/Chem	r	Observation	WRF/Chem	r
SO ₄ (µg/m ³)	3.1±2.4 (19%)	3.2±2.1 (24%)	0.39	2.6±2.0 (29%)	2.5±1.2 (38%)	0.23
NO ₃ (µg/m ³)	4.5±5.4 (28%)	4.6±5.1 (34%)	0.47	1.3±3.0 (14%)	1.5±2.7 (23%)	0.44
NH ₄ (µg/m ³)	2.6±2.2 (16%)	2.4±2.1 (19%)	0.43	1.4±1.5 (16%)	1.2±1.2 (19%)	0.42
OM (µg/m ³)	6.1±5.8 (37%)	3.0±2.6 (23%)	0.67	3.7±4.5 (41%)	1.3±1.4 (20%)	0.52
PM _{2.5} (µg/m ³)	23±13	16±10	0.75	19±17	12±9	0.80
CN (10 ³ #/cm ³)	6.7±5.0	9.4±5.4	0.40	1.0±1.1	1.7±2.8	0.74
CCN (10 ³ #/cm ³)	0.6±0.5	0.9±0.8	0.45	0.3±0.3	0.3±0.3	0.73

5

1

2 Table 4. MODIS and modelled mean values and standard deviations of droplet effective radius at
3 cloud top, liquid cloud water path and liquid cloud optical thickness, on 17-19, 25-27, and 28-30
4 May 2008.

	R _e (μm)			LWP (g/m2)			COT		
	MODIS	CTRL	NOSOA	MODIS	CTRL	NOSOA	MODIS	CTRL	NOSOA
17-19 May	10.2±3.5	7.5±3.5	8.5±4.3	230±343	242±343	208±352	32±22	33±33	21±24
25-27 May	13.7±3.7	9.1±4.4	9.8±4.9	200±166	256±502	273±480	22±19	23±30	21±27
28-30 May	10.7±3.9	8.4±4.1	7.8±3.6	141±128	224±327	243±447	19±14	27±27	24±30

5

1

2 Table 5. MODIS and modelled mean values and standard deviations of cloud water path and cloud
 3 optical thickness of clouds in all phases, on 17-19, 25-27, and 28-30 May 2008.

	CWP (g/m ²)			COT		
	MODIS-Aqua	CTRL	NOSOA	MODIS-Aqua	CTRL	NOSOA
17-19 May	207±203	336±531	218±359	26±20	30±33	19±23
25-27 May	235±182	331±533	244±418	21±16	17±23	16±21
28-30 May	206±201	370±714	262±523	21±16	24±26	21±27

4

5

FIGURES

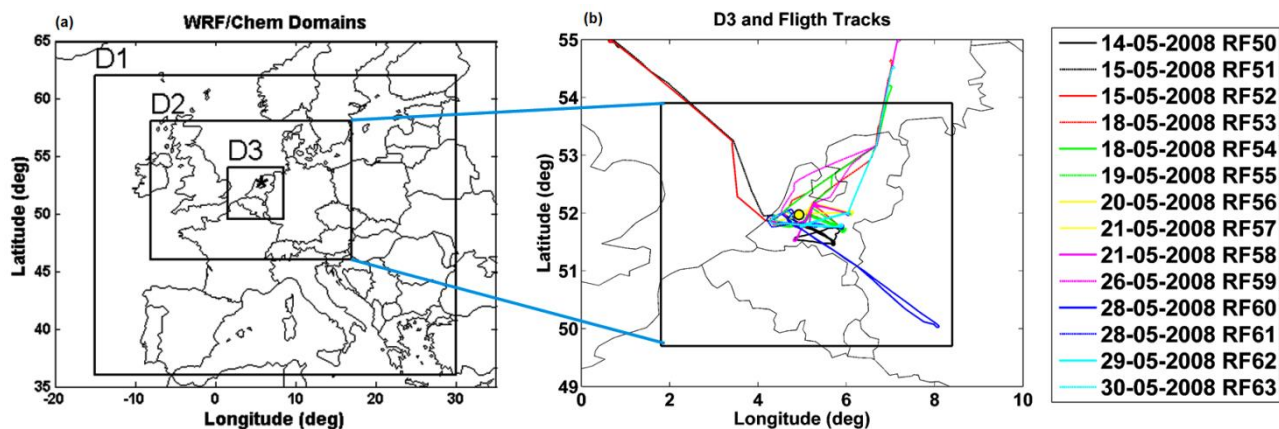


Figure 1. Panel (a) shows the three nested model domains used for simulations. D1 is 30 km resolution, D2 10 km, and D3 2 km. The black star indicates the Cabauw supersite. Panel (b) is a zoom of D3 and shows the track of every flights used in this study, yellow circle represents Cabauw supersite.

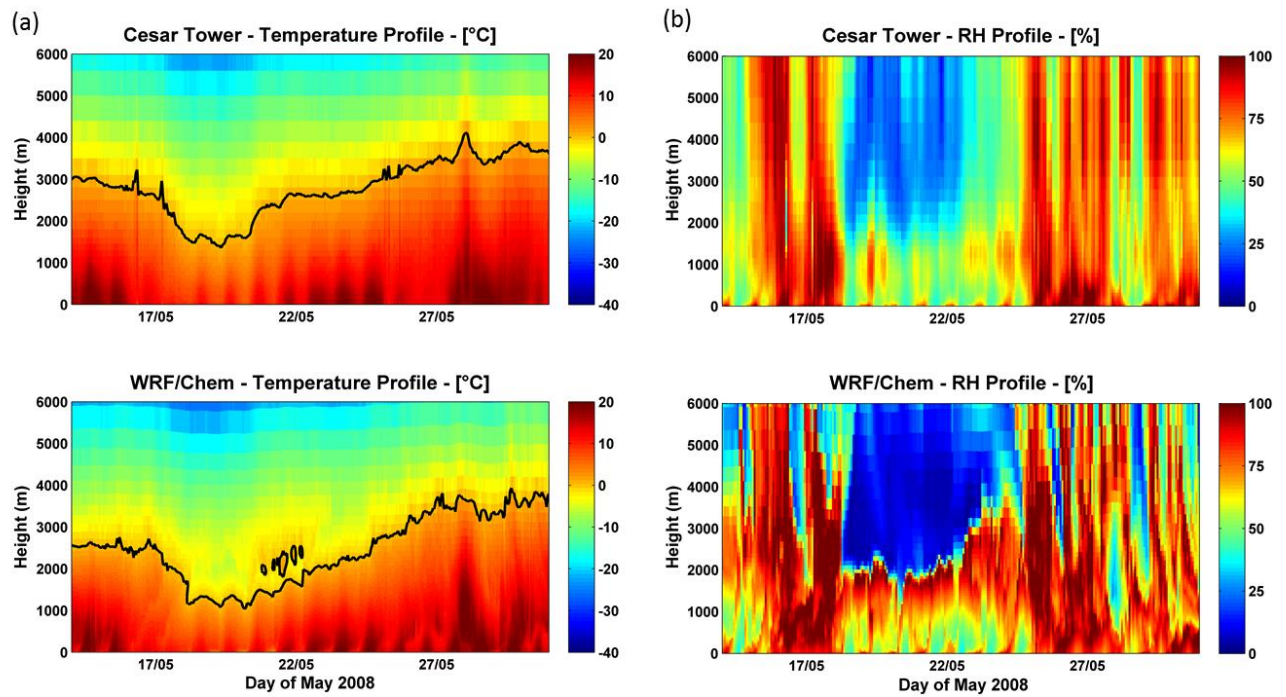
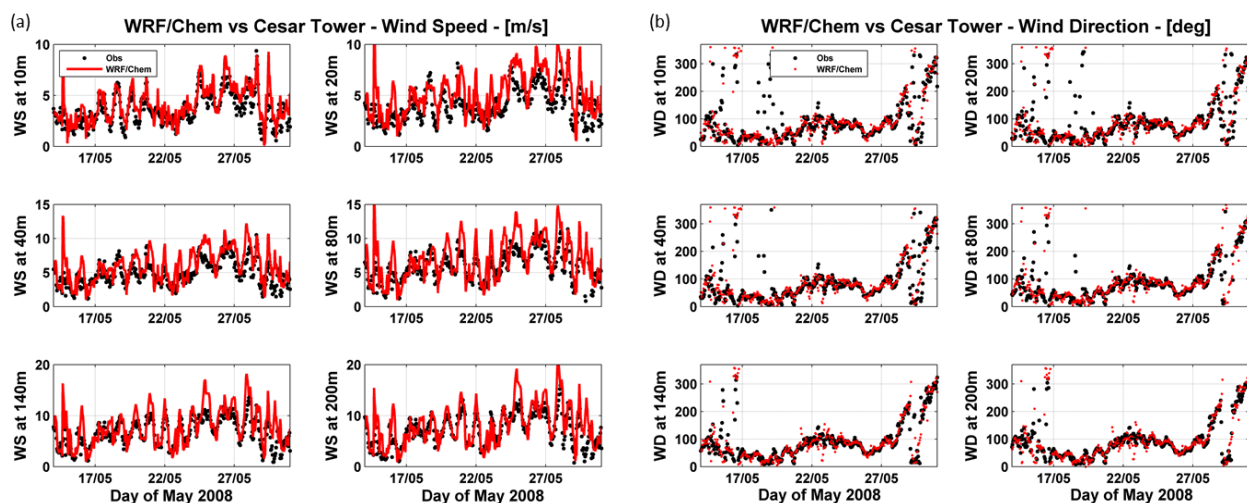


Figure 2. Observed and simulated time series of vertical profile of the temperature (a) and relative humidity (b), observed at Cesar observatory. The black line on the temperature profile represents the 0°C isotherm.

1

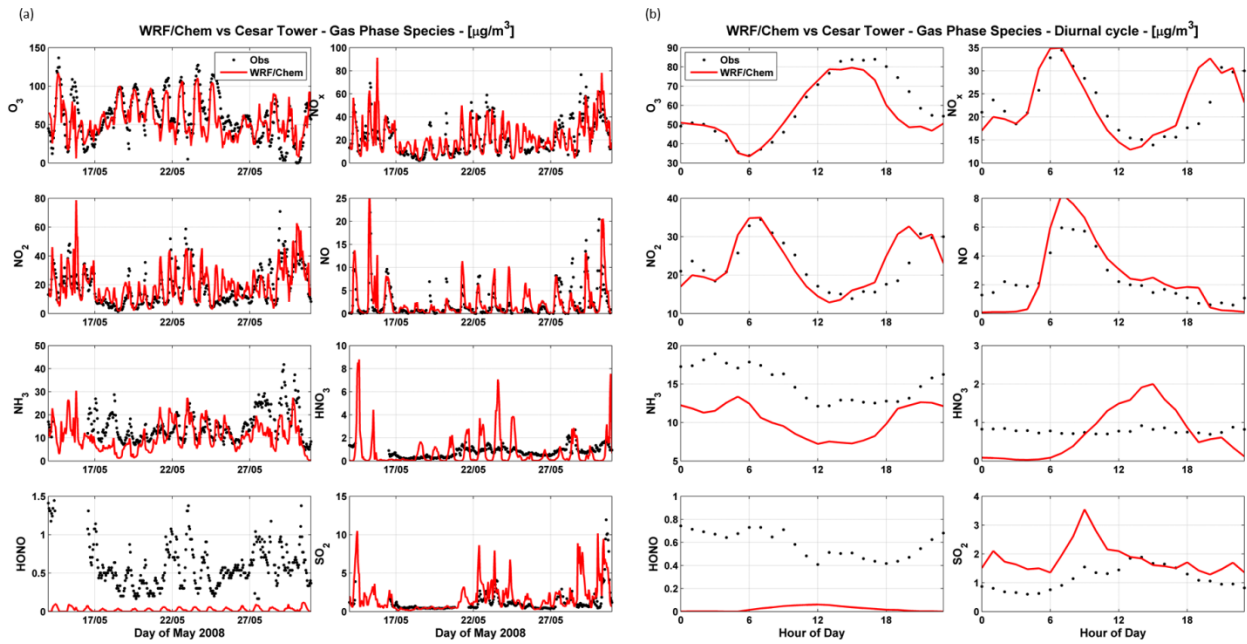


2

3 Figure 3. Observed (black lines) at Cesar Tower and simulated (red lines) time series of wind speed
 4 (a) and wind direction (b) at different height.

5

1

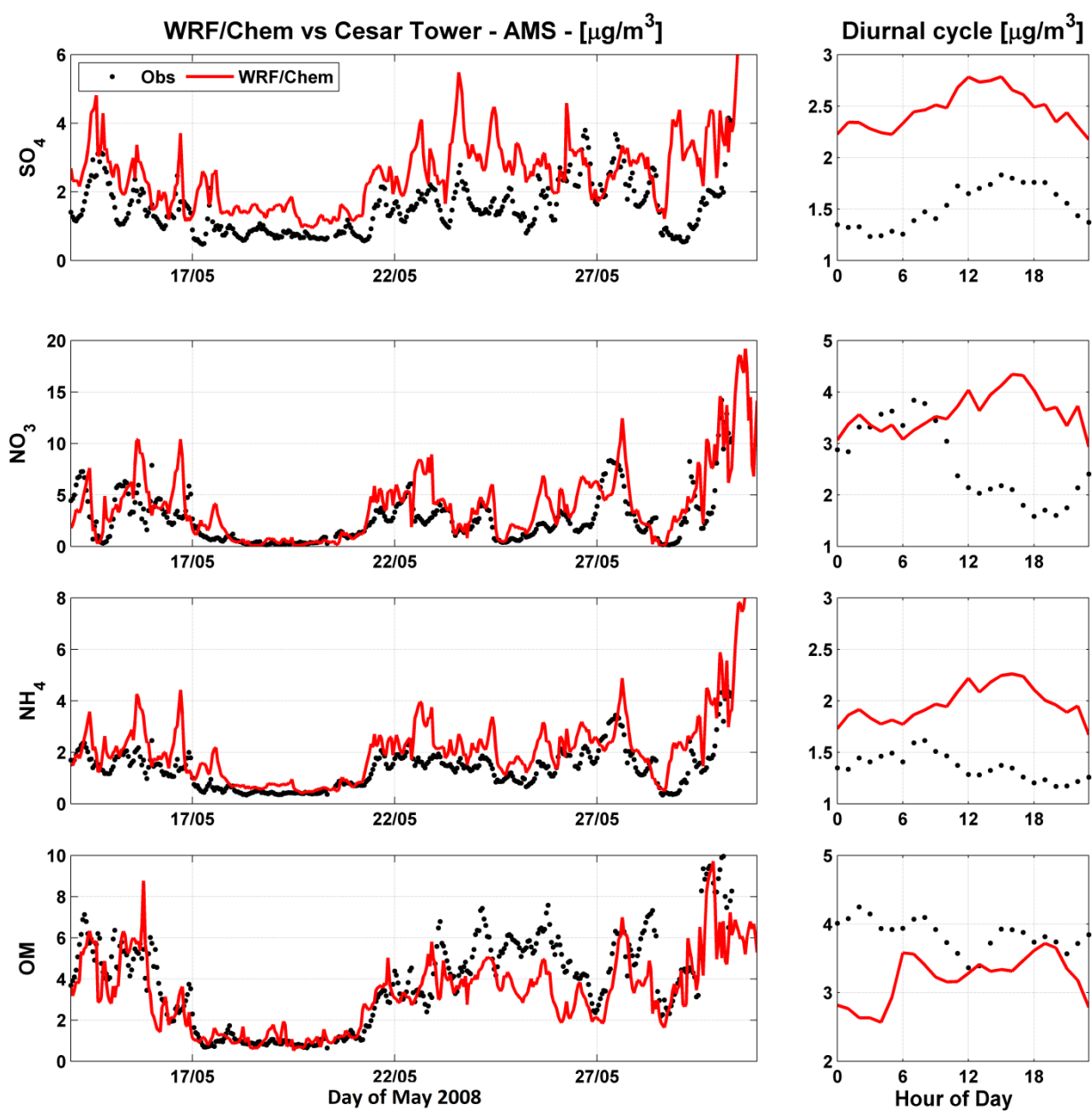


2

3 Figure 4. Observed and simulated time series of gas-phase species (a) and their average diurnal
 4 cycle (b), at Cabauw Zijdeweg EMEP station (NL0011R).

5

1



2

3 Figure 5. As Figure 4, but for aerosol mass speciation at Cesar Observatory observed at 60m height.

4

5

1

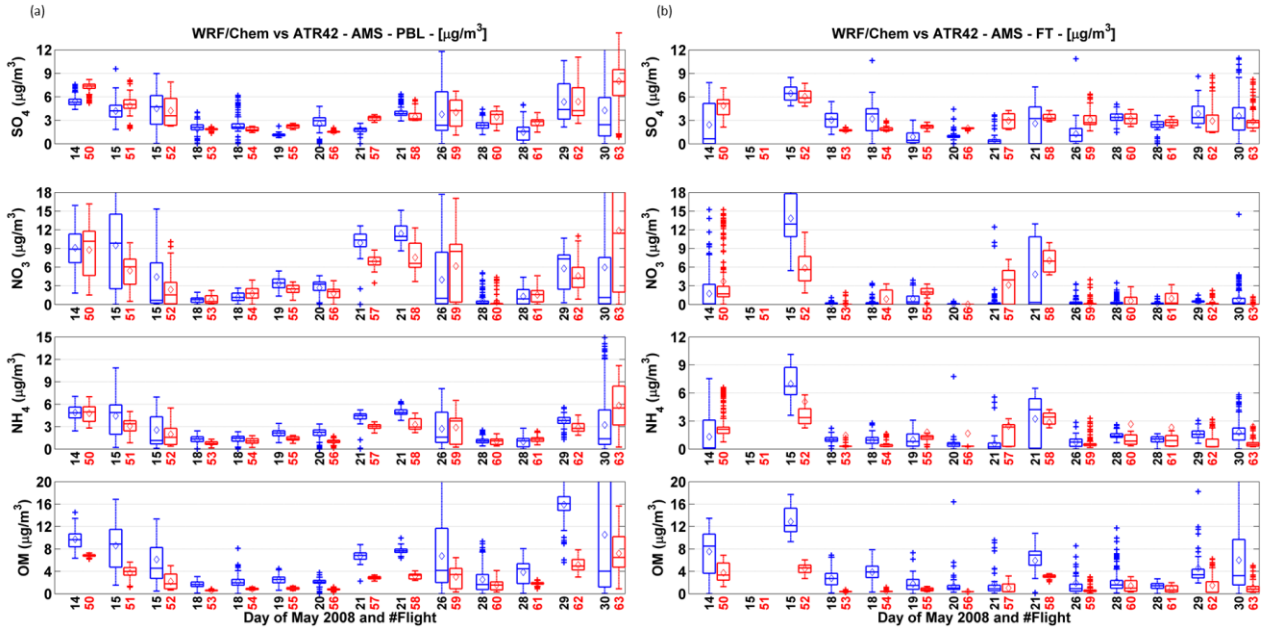
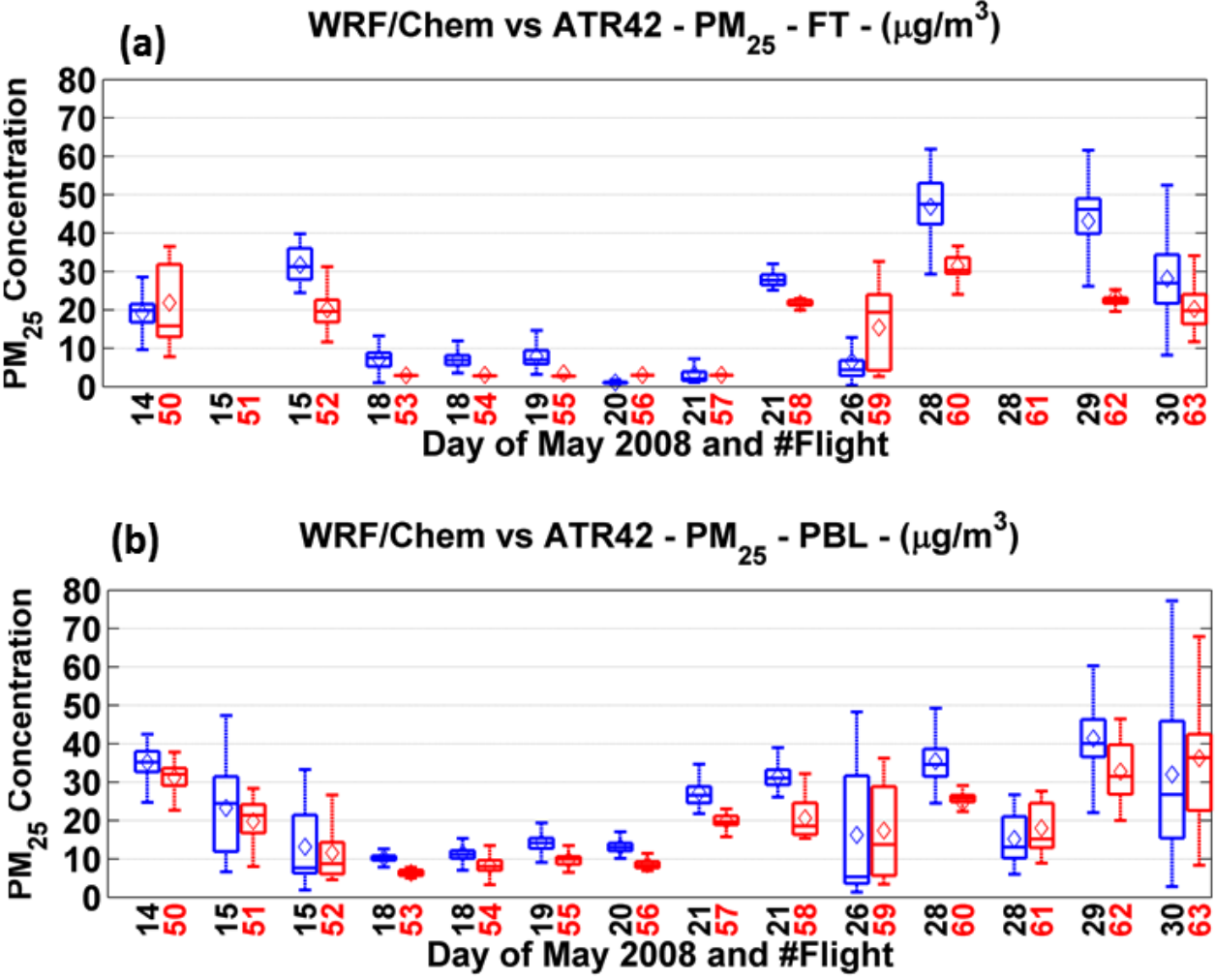


Figure 6. Box plot of SO_4 , NO_3 , NH_4 , and OM mass concentrations measured by AMS aboard the ATR-42 (blue) and simulated by WRF/Chem (red) within boundary layer (panel a) and free troposphere (panel b). The x-axis reports the day of May 2008 (black) and the number of the research flight (red). The whisker plots denote median, 25th and 75th percentiles, $1.5 \times$ (inter-quartile range), and outliers. The squares represent the mean values.

1

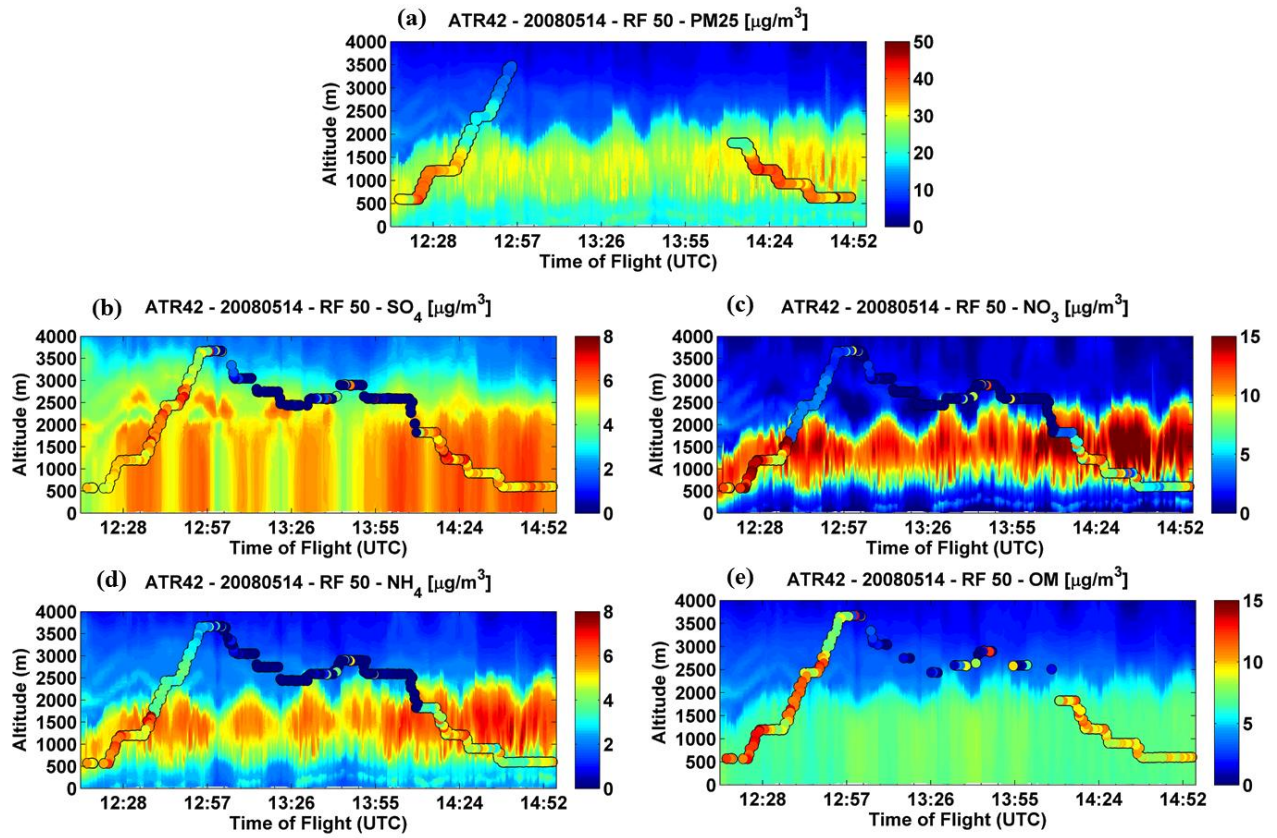


2

3 Figure 7. Same as Figure 6 but for observed and simulated PM_{2.5} mass concentrations. The blue
4 colour represents the observations will the model is displayed in red colour.

5

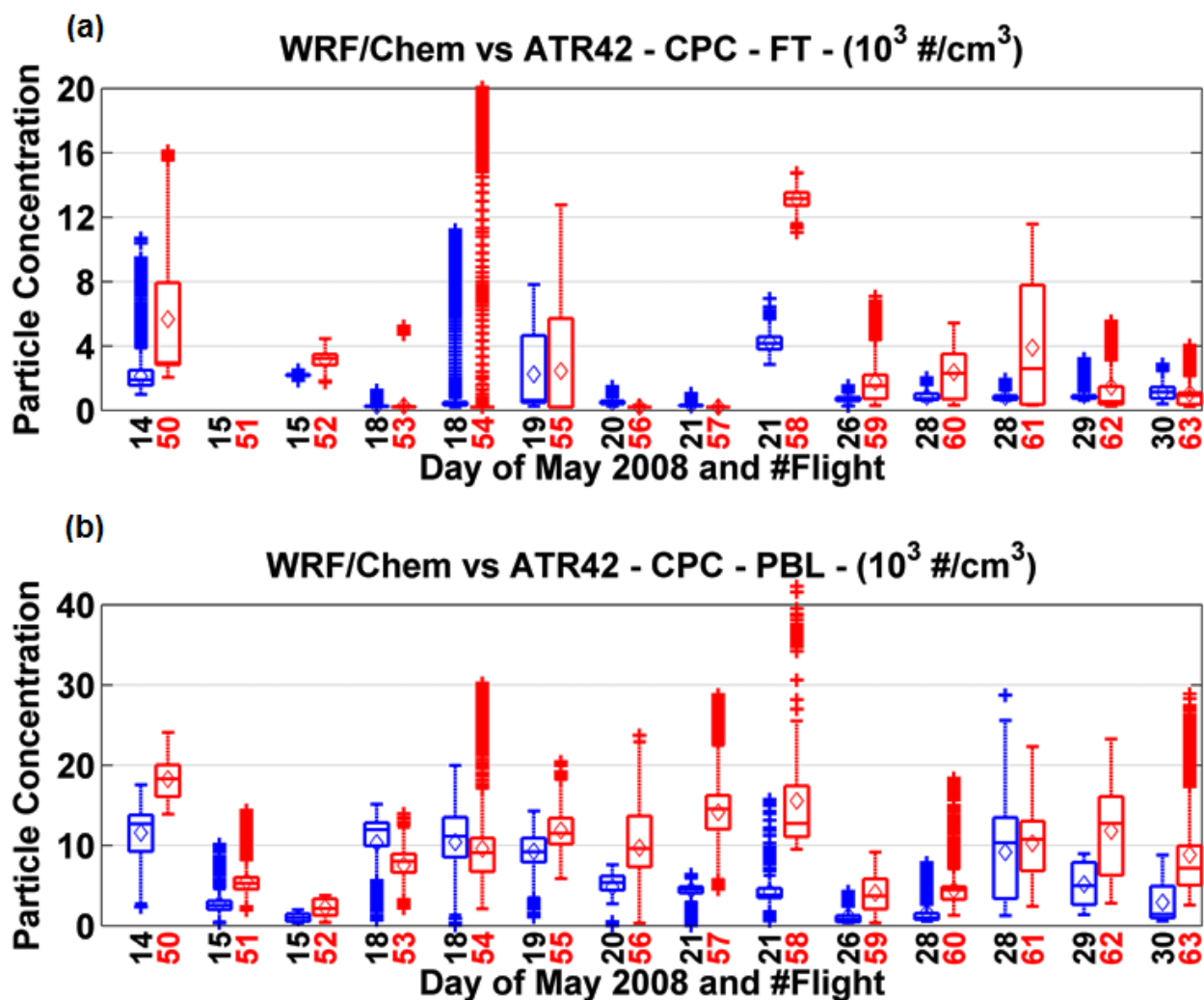
1



2

3 Figure 8. Vertical profiles (shadow) along the flight track of 14 May (RF50) of modelled PM_{2.5} (a),
 4 SO₄ (b), NO₃ (c), NH₄ (d), and OM (e). The circles are the measurements collected aboard the
 5 ATR42.

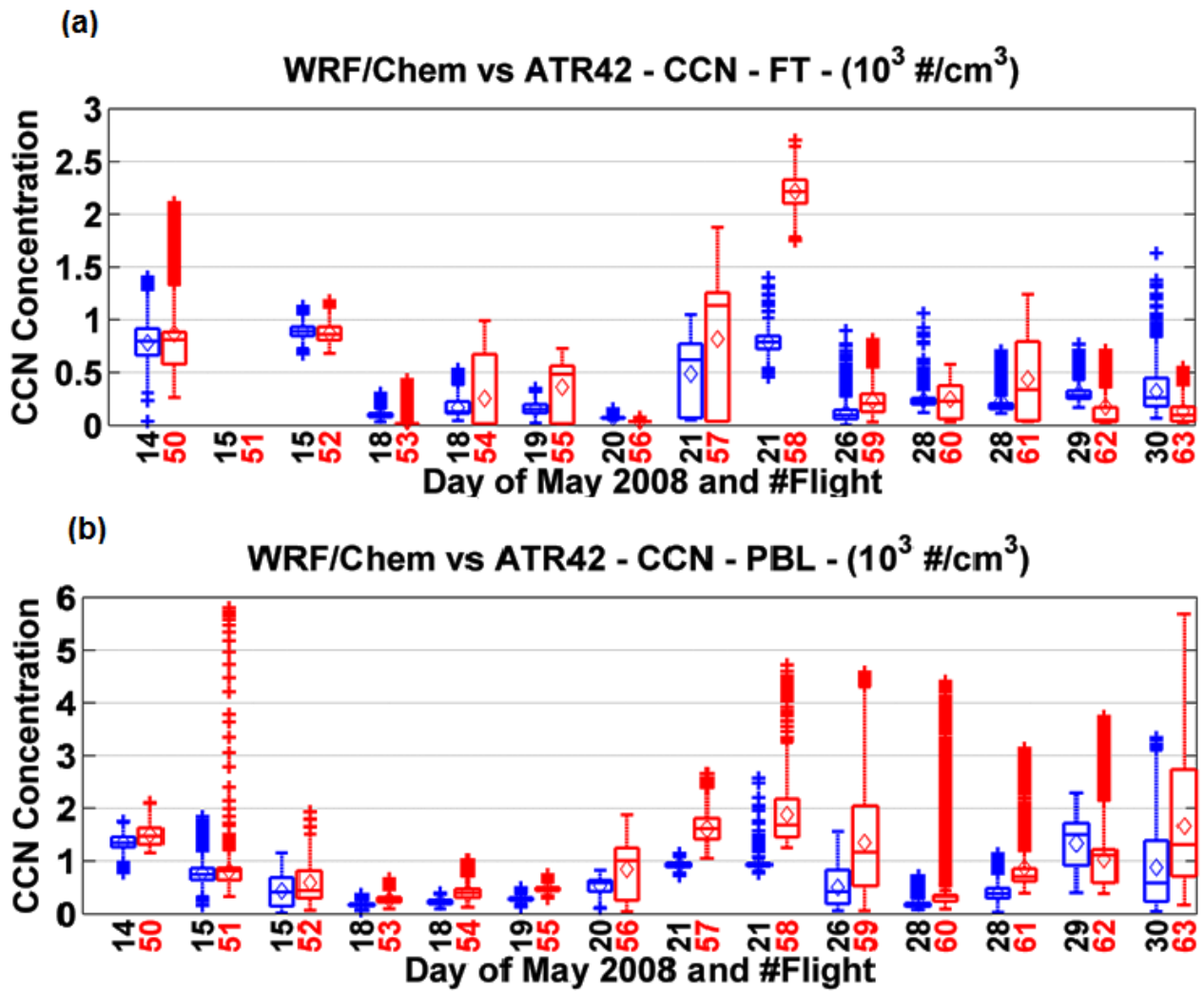
1



2
3
4
5
6
7

Figure 9. Same as Figure 6 but for observed and simulated condensation nuclei (CN) concentrations. The blue colour represents the observations while the model is displayed in red colour.

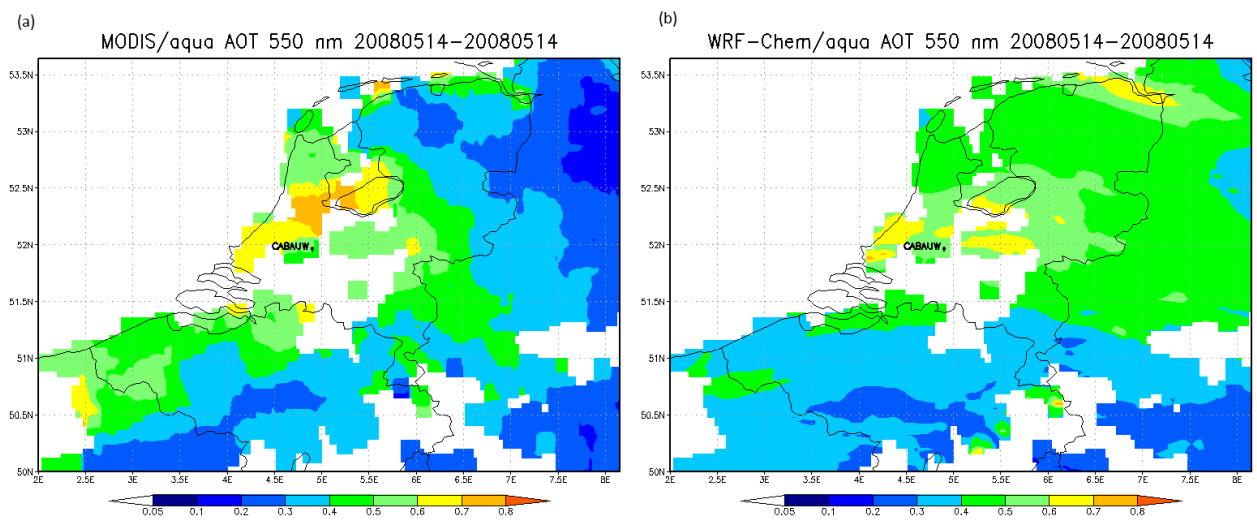
1



2
3 Figure 10. Same as Figure 6 but for observed and simulated cloud condensation nuclei (CCN)
4 concentrations at 0.2% of supersaturation. The blue colour represents the observations, the model is
5 displayed in red color.

6

1



2

3

4

5

6

Figure 11. Aerosol optical thickness at 500 nm from MODIS-Aqua (panel a) and WRF/Chem simulations (panel b) on 14 May 2008.

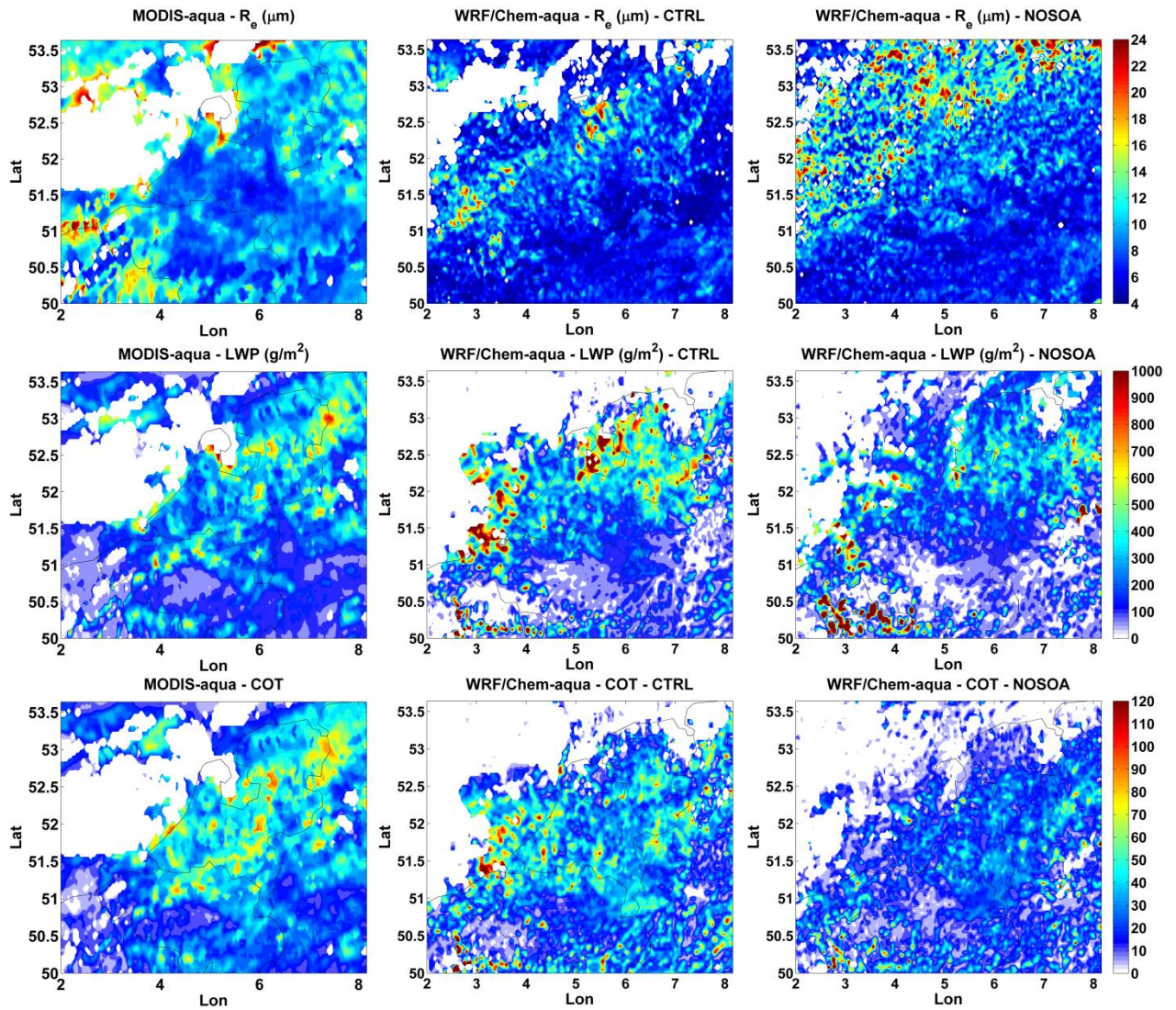
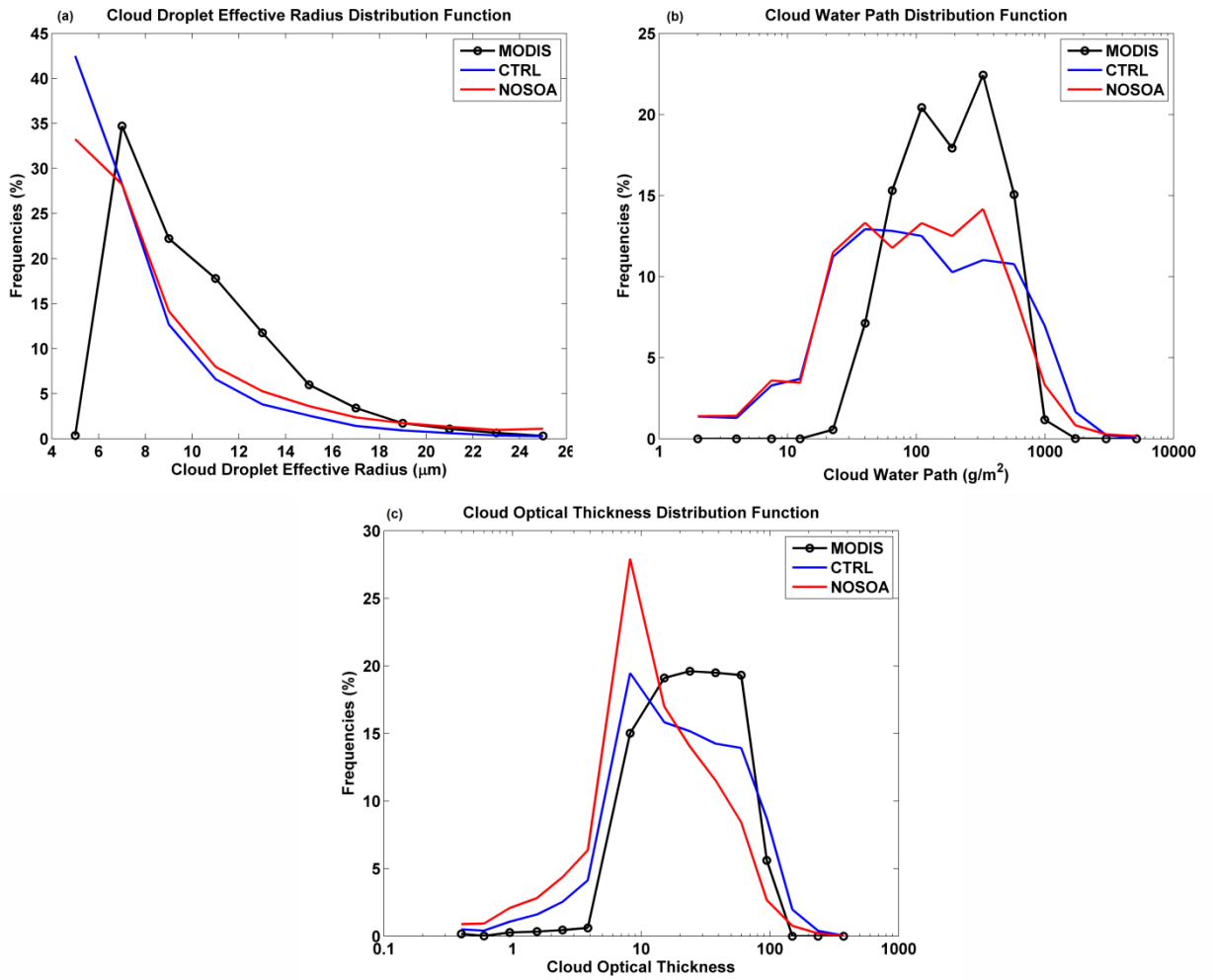


Figure 12. 17-19 May 2008 averages of droplet effective radius at cloud top (first row), liquid water path (second row), and liquid cloud optical thickness (third row), retrieved using MODIS-aqua observations (first column), predicted by model in the references run (CTRL, second columns) and sensitivity test without SOA (NOSOA, third column).

1

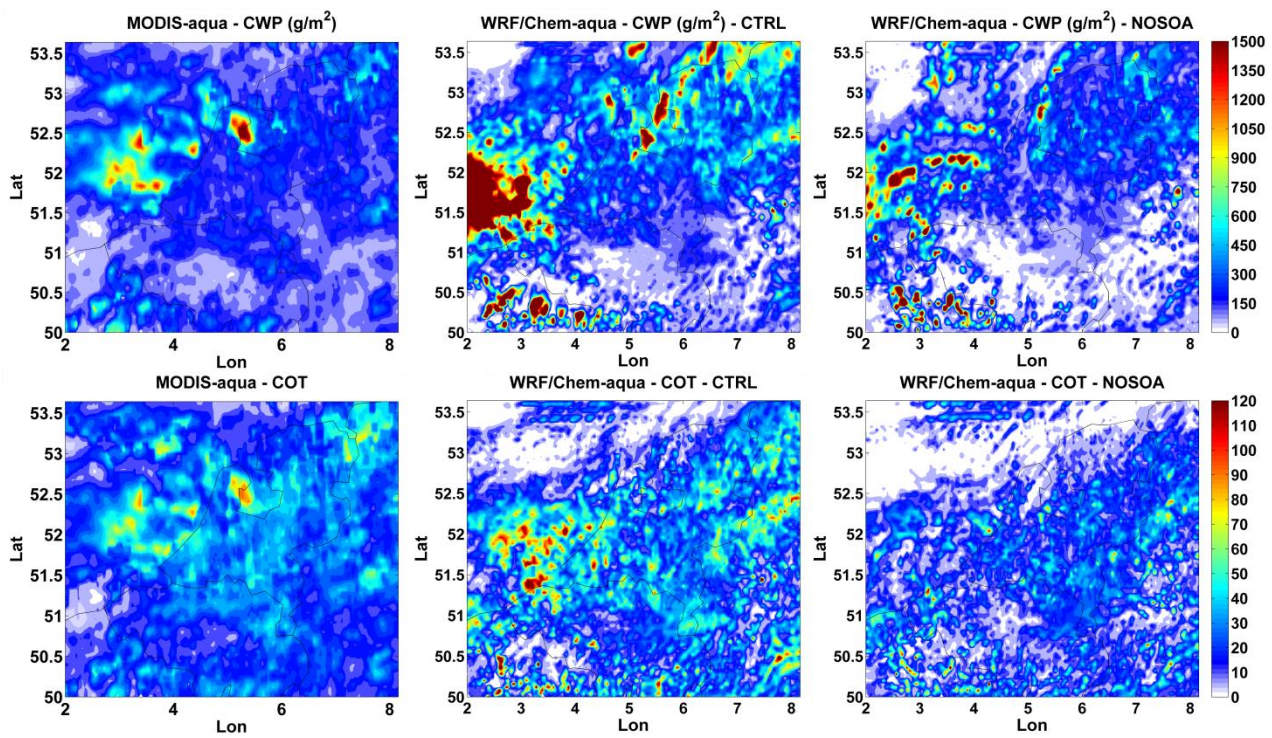


2

3 Figure 13. 17-19 May 2008 averages of observed and simulated distribution function of droplet
 4 effective radius at cloud top (a), liquid water path (b) and liquid cloud optical thickness (c). The
 5 black line represents the observations retrieved by MODIS, blue and red colours correspond to
 6 model predictions from the reference run (CTRL) and sensitivity test without SOA (NOSOA),
 7 respectively.

8

1



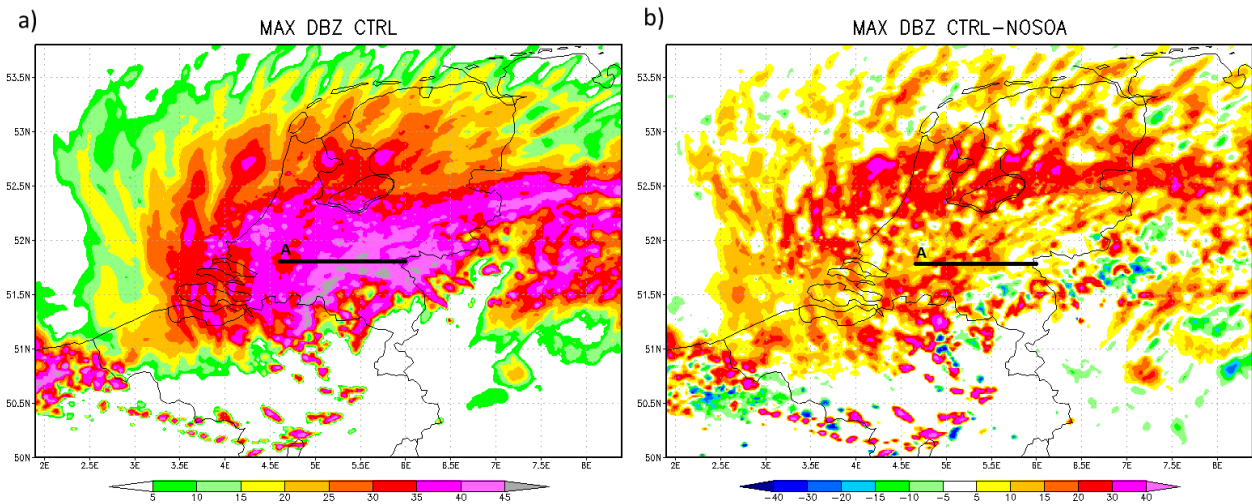
2

3

4 Figure 14. As Figure 12, but for clouds in mixed phase.

5

1



2

3 Figure 15. Maximum dBZ at 6 UTC of 17 May for CTRL run (a) and difference of maximum dBZ
 4 between CTRL and NOSOA simulations (b). The solid black line represents the cross section A
 5 used to plot vertical profiles reported in Figure 13.

6

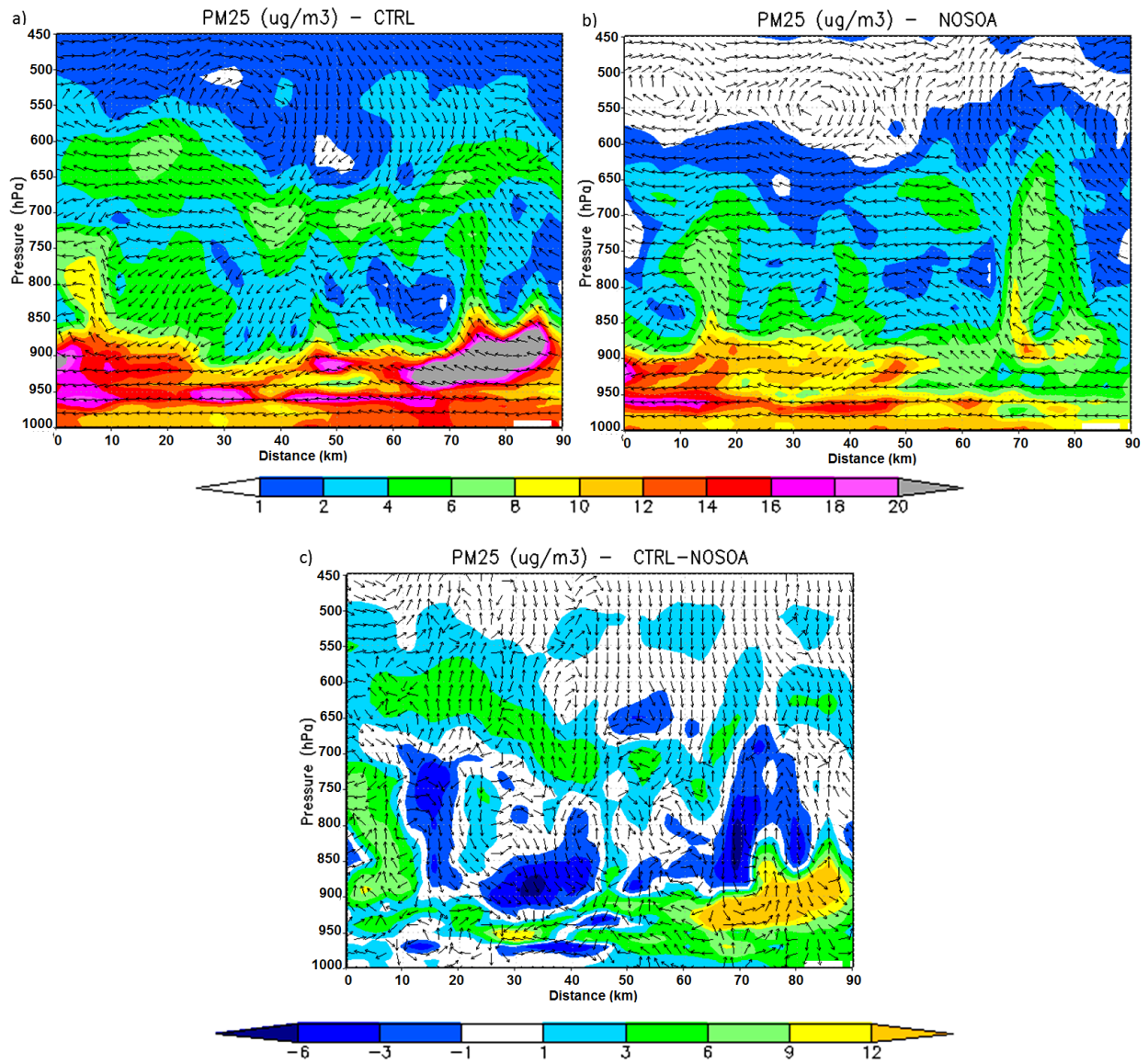
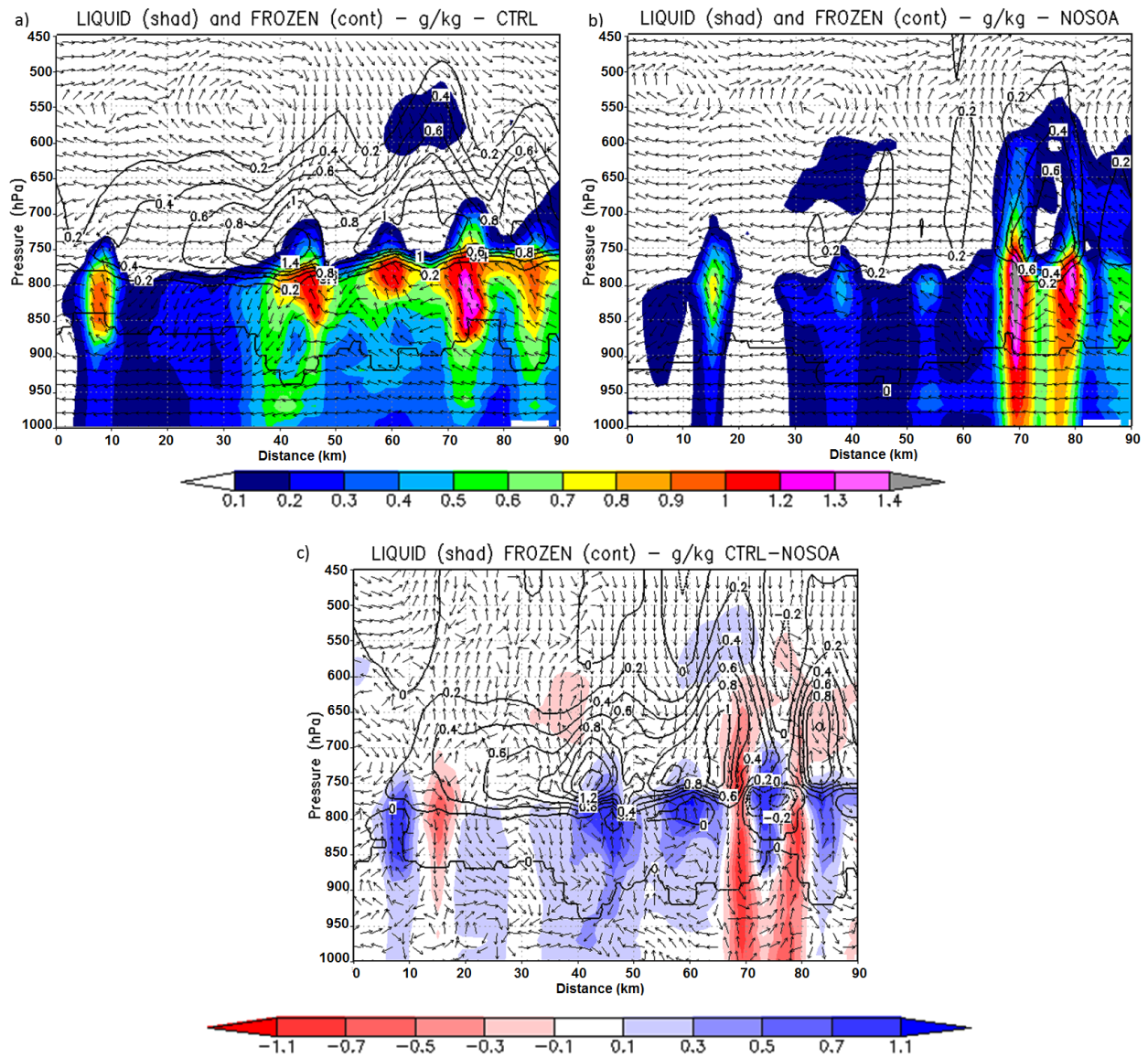


Figure 16. Vertical profile of PM2.5 mass (color) and wind (vector) for CTRL run (a), NOSOA run (b) and their differences (c). The fields are extracted along the cross section A (see Figure 12) at 6 UTC of 17 May. The x-axis reports the west-east distance in km along the cross section.

1



2

3 Figure 17. As Figure 16, but for water (color), and frozen (black contours) hydrometeors.

4